Earth and Planetary Science Letters 297 (2010) 211–225

Contents lists available at ScienceDirect

Earth and Planetary Science Letters

journal homepage: www.elsevier.com/locate/epsl

Regolith production rates calculated with uranium-series isotopes at Susquehanna/Shale Hills Critical Zone Observatory

Lin Ma [a,*], Francois Chabaux [b], Eric Pelt [b], Estelle Blaes [b], Lixin Jin [a], Susan Brantley [a]

[a] Earth and Environmental Systems Institute, Pennsylvania State University, University Park, PA 16802, USA
[b] Laboratoire d'Hydrologie et de Geochimie de Strasbourg, EOST, University of Strasbourg and CNRS, Strasbourg, France

ARTICLE INFO

Article history:
Received 20 December 2009
Received in revised form 3 June 2010
Accepted 12 June 2010
Available online 7 July 2010

Editor: M.L. Delaney

Keywords:
U-series isotopes
regolith formation
chemical weathering
erosion
critical zone

ABSTRACT

In the Critical Zone where rocks and life interact, bedrock equilibrates to Earth surface conditions, transforming to regolith. The factors that control the rates and mechanisms of formation of regolith, defined here as material that can be augered, are still not fully understood. To quantify regolith formation rates on shale lithology, we measured uranium-series (U-series) isotopes (^{238}U, ^{234}U, and ^{230}Th) in three weathering profiles along a planar hillslope at the Susquehanna/Shale Hills Observatory (SSHO) in central Pennsylvania. All regolith samples show significant U-series disequilibrium: (^{234}U/^{238}U) and (^{230}Th/^{238}U) activity ratios range from 0.934 to 1.072 and from 0.903 to 1.096, respectively. These values display depth trends that are consistent with fractionation of U-series isotopes during chemical weathering and element transport, i.e., the relative mobility decreases in the order ^{234}U>^{238}U>^{230}Th. The activity ratios observed in the regolith samples are explained by i) loss of U-series isotopes during water–rock interactions and ii) re-deposition of U-series isotopes downslope. Loss of U and Th initiates in the meter-thick zone of "bedrock" that cannot be augered but that nonetheless consists of up to 40% clay/silt/sand inferred to have lost K, Mg, Al, and Fe. Apparent equivalent regolith production rates calculated with these isotopes for these profiles decrease exponentially from 45 m/Myr to 17 m/Myr, with increasing regolith thickness from the ridge top to the valley floor. With increasing distance from the ridge top toward the valley, apparent equivalent regolith residence times increase from 7 kyr to 40 kyr. Given that the SSHO experienced peri-glacial climate ~15 kyr ago and has a catchment-wide averaged erosion rate of ~15 m/Myr as inferred from cosmogenic ^{10}Be, we conclude that the hillslope retains regolith formed before the peri-glacial period and is not at geomorphologic steady state. Both chemical weathering reactions of clay minerals and translocation of fine particles/colloids are shown to contribute to mass loss of U and Th from the regolith, consistent with major element data at SSHO. This research documents a case study where U-series isotopes are used to constrain the time scales of chemical weathering and regolith production rates. Regolith production rates at the SSHO should be useful as a reference value for future work at other weathering localities.

1. Introduction

Bedrock is converted to erodible regolith through physical, chemical, biological and hydrological processes operating together within the thin layer at Earth's surface – the Critical Zone – where rocks, vegetation, atmospheric gases and water interact (e.g., White et al., 1996; Heimsath et al., 1997; Anderson et al., 2002; Amundson, 2004; Brantley et al., 2007a; Brantley and White, 2009). Over time, the bedrock–regolith interface (the weathering front) propagates downward into the bedrock. The balance between rates of erosion and regolith production contribute to both the regolith thickness and the overall landscape morphology (Carson and Kirkby, 1972; Stallard, 1992; Heimsath et al., 1997; Minasny and McBratney, 1999). Furthermore, the products of weathering, regolith, are vital for the sustainability of ecosystems and human society (Montgomery, 2007; Porder et al., 2007; Brantley, 2008). Human activities have resulted in a sharp increase in rates of continental erosion and sedimentation (Wilkinson and McElroy, 2007). It is currently of great importance to predict how regolith will respond to anthropogenic and climate perturbations. However, the factors that control the rates and mechanisms of regolith formation are still not fully understood.

Chemical weathering of bedrock mobilizes elements from the lithosphere, providing nutrients to the biosphere, controlling river and ocean chemistry in the hydrosphere, as well as regulating CO_2 and global climate for the atmosphere (e.g., Kump et al., 2000; Drever, 2004; Godderis et al., 2009). Detailed chemical analyses and models of chemical mass balance have been routinely used to study chemical and physical changes during regolith formation (Brimhall and Dietrich, 1987; Taylor and Blum, 1995; White and Blum, 1995; Murphy et al., 1998; White et al., 1998; Amundson, 2004; Lebedeva et al., 2007; Yoo et al., 2007; Steefel,

* Corresponding author. Tel.: +1 814 863 8055.
E-mail address: lxm59@psu.edu (L. Ma).

0012-821X/$ – see front matter © 2010 Elsevier B.V. All rights reserved.
doi:10.1016/j.epsl.2010.06.022

2008; Brantley and White, 2009). Such approaches generally require independent estimates of the regolith production rates. Cosmogenic isotopes (e.g., ^{10}Be and ^{26}Al) have been used to provide estimates of total denudation rates (e.g., Lal, 1991; Bierman and Nichols, 2004; von Blanckenburg, 2005). From these denudation rates, soil production rates can be inferred if soil thickness is constant over time (e.g., Heimsath et al., 1997; Small et al., 1999; Riebe et al., 2003). However, such an assumption is generally difficult to evaluate and has only been tested in a few instances (e.g., Heimsath et al., 1997,2000; Dosseto et al., 2008b).

Uranium-series (U-series) isotopes (e.g., ^{238}U, ^{234}U and ^{230}Th) offer a powerful tool to investigate regolith production rates or residence times in a weathering system. ^{238}U decays with a halflife ($T_{1/2}$) of ~4.5 Gyr to produce ^{234}U ($T_{1/2}$ = 244 kyr), which in turn decays to ^{230}Th ($T_{1/2}$ = 75 kyr). For a system closed to inputs or outputs of U-series isotopes for longer than ~1.3 Myr, these isotopes will be in secular equilibrium (i.e., daughter/parent activity ratios equal unity). However, U is soluble in water while Th is "particle-reactive", i.e., it generally associates with solid surfaces (Langmuir, 1978; Langmuir and Herman, 1980). Importantly, compared with ^{238}U, ^{234}U is released to solution to great extent because ^{234}U is produced by alpha particle emission from ^{238}U and this heavy particle often damages the crystal lattice enabling preferential loss of the lighter isotope during water–rock interaction (Fleischer, 1980). In other words, congruent dissolution of U-containing materials releases both isotopes equivalently to solution but ^{234}U can also be released preferentially to solution because of the alpha particle effect. Because of these reasons, the relative mobility of U-series isotopes during weathering is believed to be ^{234}U>^{238}U>^{230}Th (e.g., Rosholt et al., 1966; Latham and Schwarcz, 1987a,b; Vigier et al., 2001; Chabaux et al., 2003a,2008; Dosseto et al., 2008a). Therefore, fluid phases are generally characterized by (^{234}U/^{238}U)>1 and (^{230}Th/^{238}U)<1 (parenthesis means activity ratio hereafter), while materials that have weathered recently generally show (^{234}U/^{238}U)<1 and (^{230}Th/^{238}U)>1. The amount of disequilibrium in the weathering residual depends on both the extent and duration of weathering processes. In particular, the disequilibrium tracks the development of mineral–water interfacial area for the major U-bearing phases. Hence, U-series isotopes have been used to place time constraints on the initiation and duration of chemical weathering over a wide range of spatial scales, including ocean sediment cores, weathering profiles and rinds, shallow aquifers, small river catchments, and large drainage basins (e.g., Gascoyne, 1992; Plater et al., 1994; Mathieu et al., 1995; Vigier et al., 2001; Dequincey et al., 2002; Chabaux et al., 2003a,b; Maher et al., 2004; Vigier et al., 2005; Chabaux et al., 2006; Depaolo et al., 2006; Dosseto et al., 2006a,b,c; Vigier et al., 2006; Granet et al., 2007; Chabaux et al., 2008; Dosseto et al., 2008a,b; Gaillardet, 2008; Pelt et al., 2008; Bourdon et al., 2009).

Here, we present a study of U-series isotopes in regolith profiles developed on shale bedrock at the Shale Hills catchment, an observatory established in central Pennsylvania as a part of a network of observatories to investigate Earth surface processes related to hydrology, geochemistry, ecology, and geomorphology within the Critical Zone (Brantley et al., 2007b). We show here that the regolith samples display significant U-series disequilibrium resulted from shale weathering processes. By using U-series isotopes, we determine the time scales of shale weathering and regolith production rates for this experimental watershed. The mobility behavior of U-series isotopes during weathering is also systematically investigated in this Critical Zone observatory. The success of this method in estimating rates of regolith formation also enhances our ability to use this technique in other environments to understand the response of regolith productions to climate perturbations.

2. Methods

2.1. Site description

Shale has been the focus of some pioneering weathering studies (Littke et al., 1991; Kolowith and Berner, 2002; Piersson-Wickmann et al., 2002; Copard et al., 2007; Tuttle and Breit, 2009; Tuttle et al., 2009), as it covers about 25% of the land surface area (Amiotte-Suchet et al., 2003). Weathering of shale controls global geochemical fluxes of C, P, and Pt-group elements (Petsch et al., 2001; Kolowith and Berner, 2002; Amiotte-Suchet et al., 2003). To better understand shale weathering processes, the Susquehanna/Shale Hills Observatory (SSHO) is established in central Pennsylvania (Fig. 1a). This 8-hectare watershed is managed as a Pennsylvania State University experimental forest. Extensive field studies have been conducted at SSHO from forestry field experiments, global information system (GIS) and digital elevation models, soil moisture synoptic sampling, soil mapping, stream flow monitoring, and ongoing geophysics and geochemical observations (Lynch, 1976; Lynch and Corbett, 1985; Duffy and Cusumano, 1998; Lin et al., 2006; Qu and Duffy, 2007; Jin et al., 2010). As such, SSHO is an ideal site to study the fractionation of U-series isotopes during water–rock interactions.

At SSHO, the mean annual temperature is 10 °C and the mean annual precipitation is 107 cm (NOAA, 2007). A 1st-order stream flows within the catchment and eventually joins the Susquehanna River (Fig. 1a). The V-shaped catchment is characterized by an average E–W channel and average local relief of 30 m (Lynch, 1976; Lin, 2006). The hillslopes are covered with deciduous trees (maple, oak, and beech) and the valley is covered by hemlocks and pines (Lin, 2006).

The SSHO has developed almost entirely upon Rose Hill Formation (Folk, 1960; Lynch, 1976; Lynch and Corbett, 1985). The 700-foot-thick Silurian-age formation consists of olive-pink, grayish-buff shales with a few interbedded limestones (Lynch, 1976). The shale bedrock is composed predominantly of illite (58 wt.%), quartz (30 wt.%), "vermiculited" chlorite (11 wt.%), and trace feldspar (plagioclase and K-feldspar), anatase (TiO_2), Fe-oxides (magnetite and hematite) and zircon (Jin et al., 2010). Chemical weathering reactions in the regolith at SSHO are dominated by clay transformations wherein illite, "chlorite", and plagioclase weather to a vermiculite phase and kaolinite. The regolith is defined here to be the zone that can be augered by hand. Beneath the regolith–bedrock interface, evidence is consistent with dissolution of carbonates and feldspar in the underlying rock (Jin et al., 2010). Regolith thickness averages 1.4 m over the catchment, ranging from shallow at the ridge top to much deeper in the valley floor and in topographic depressions (Fig. 1a).

Erosion rates of the Appalachian mountain region are estimated to range from 8 to 29 m/Myr (Roden and Miller, 1989; Blackmer et al., 1994; Reuter et al., 2004). One measurement of cosmogenic ^{10}Be in a stream sediment sample from SSHO shows a catchment-averaged erosion rate of 15 m/Myr (Jin et al., 2010), a value that is consistent with other shale localities in the Appalachians. However, the SSHO has experienced at least two significant perturbations in the geologically recent past: a perturbation from peri-glacial to modern conditions (~15 kyr; Gardner et al., 1991), and clearing of forests during colonial occupation. The catchment lies ~80 km south of the greatest advance of glacial ice in central Pennsylvania during the last glacial maximum (Braun, 2005).

2.2. Sample collection and U–Th isotope analyses

We focus here on the U-series isotopic compositions for previously collected samples of augered core from three sites along one planar hillslope on the southern slope of the catchment (southern planar ridge top: SPRT; southern planar middle slope: SPMS; and southern planar valley floor: SPVF). Here, fluid flow in the regolith is considered to be largely two-dimensional downslope, i.e., nonconvergent flow, and the hillslope is thus referred to as a 2-D weathering profile (Fig. 1). These compositions are compared to relatively unaltered "parent materials" obtained by drilling into the underlying bedrock (see further discussion below). The drilled core was obtained as powdered sample using a rotary air drill in the northern ridge of the catchment (Fig. 1a).

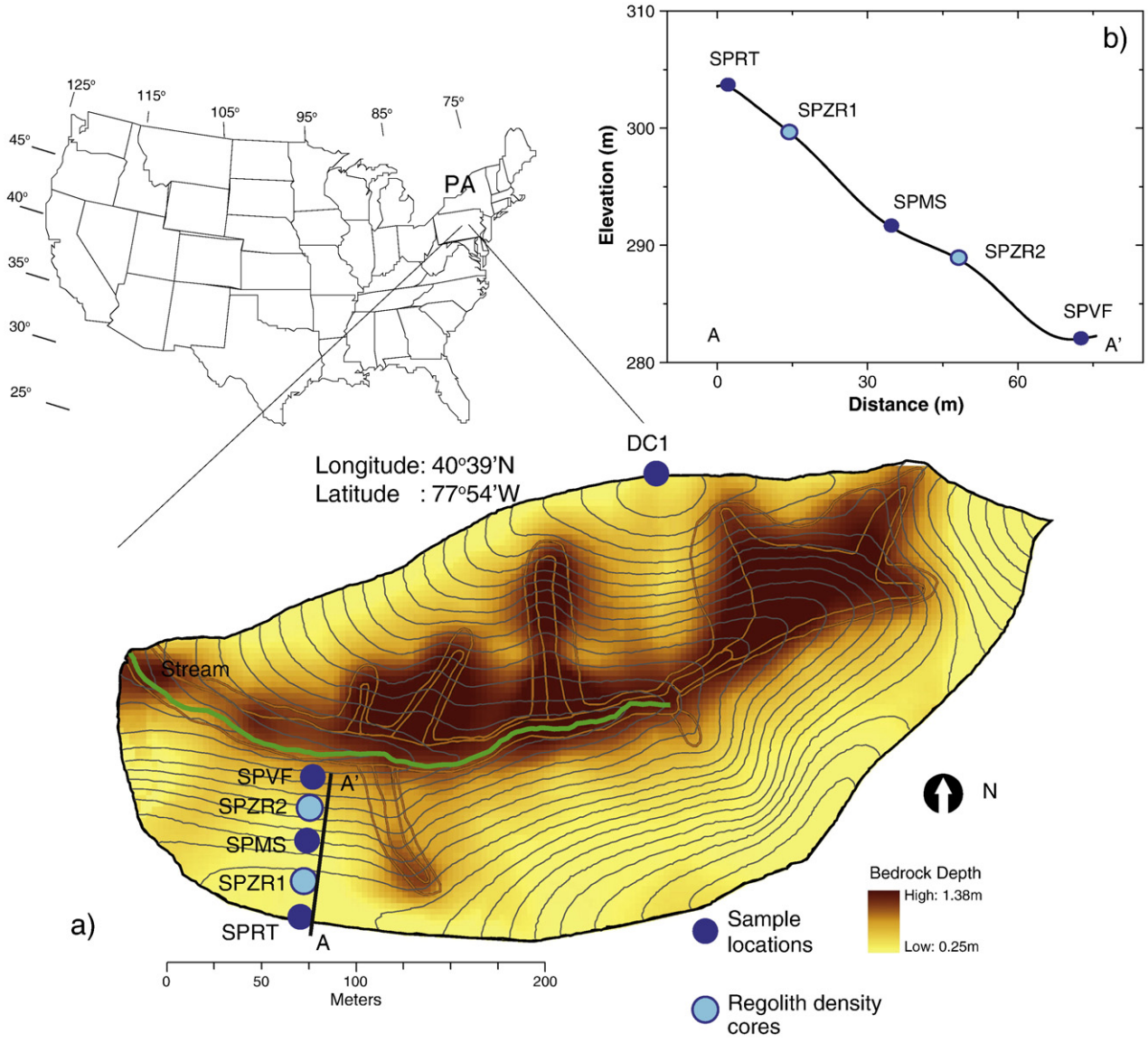

Fig. 1. a) Regolith sample locations in the Shale Hills catchment (modified after Lin et al., 2006). Background color indicates regolith thickness; yellow lines indicate the outlines of the five previously identified soil series (Lin et al., 2006); grey lines indicate topographic contours. DC1 is the drill core site where 24 m of parent shale was sampled as chips (Jin et al., 2010). Regolith cores SPRT, SPMS, and SPVF comprise a 2D planar transect (black line: A–A′). Two regolith cores (SPZR1 and SPZR2) sampled along the hillslope for bulk density analyses are also indicated; b) Cross section of the 2D planar transect (A–A′): notice that the surface varies from flat at SPRT, to linear at SPMS, to concave at SPVF.

Regolith samples were collected using a 2-inch diameter hand auger at about 10 cm intervals until refusal. Importantly, "regolith" defined here includes both the mobile layer near the surface (the "soils" or "mobile layer", e.g., Dietrich et al., 2003) and the underlying "immobile layer". "Bedrock" is here defined as fragmented or unfragmented rock that was inaccessible to the auger. The deepest regolith samples generally contained a high fraction of rock fragments. Importantly, the samples were not size-separated but rather, the entire sample of rock fragments + granular material was ground and analyzed. Zero depth was defined as the bottom of the 3-cm thick organic layer or, equivalently, the top of the mineral soil. The samples used in this study were derived as splits of the samples from the cores described previously (Jin et al., 2010).

Analyses of U and Th isotopes and concentrations were performed at the Laboratoire d'Hydrologie et de Geochimie de Strasbourg, University of Strasbourg (France), following the procedures as described in Granet et al. (2007) and Pelt et al. (2008) (see Appendix A for analytical details).

3. Results

The activity ratios and concentrations of U and Th in the regolith and bedrock samples are presented in Table 1. For splits of the same samples, regolith density, mineralogy, and mobility of major elements during chemical weathering are discussed by Jin et al. (2010).

3.1. U-series activity ratios

The Silurian-aged bedrock samples (DC1-8 and DC1-26) show values of ($^{234}U/^{238}U$) and ($^{230}Th/^{238}U$) equal to 1 within error (Table 1, Fig. 2), as expected for secular equilibrium in a rock older than 1 Ma in age, i.e., a rock that has not lost significant ^{234}U due to water–rock interaction. In contrast, regolith samples are not in secular equilibrium. ($^{234}U/^{238}U$) values measured in regolith samples from the ridge top (SPRT), middle slope (SPMS), and valley floor (SPVF) profiles range from 0.936 to 0.951, from 0.934 to 0.972, and from 0.966 to 1.072, respectively (Table 1, Fig. 2). Furthermore, all three profiles show

Table 1
U–Th concentrations and activity ratios of regolith and bedrock samples at the Shale Hills catchment.

Samples	Depth (cm)	U (ppm)	±2σ	Th (ppm)	±2σ	(^{234}U/^{238}U)a	±2σ	(^{230}Th/^{238}U)a	±2σ	(^{238}U/^{232}Th)a	±2σ	(^{230}Th/^{232}Th)a	±2σ	Zr (ppm)
SPRT0010	5	2.728	0.019	12.58	0.13	0.936	0.005	1.052	0.015	0.658	0.007	0.692	0.007	273
SPRT1020	15	2.780	0.019	12.60	0.13	0.943	0.005	1.040	0.015	0.669	0.007	0.696	0.007	275
SPRT2030	25	2.777	0.019	12.44	0.12	0.951	0.005	1.036	0.015	0.677	0.007	0.701	0.007	246
SPMS0010	5	2.733	0.019	12.56	0.13	0.934	0.005	1.096	0.015	0.660	0.007	0.723	0.007	351
SPMS1020	15	2.768	0.019	12.25	0.12	0.942	0.005	1.039	0.015	0.686	0.007	0.712	0.007	329
SPMS2030	25	2.800	0.020	12.20	0.12	0.958	0.005	1.032	0.014	0.696	0.007	0.719	0.007	295
SPMS3040	35	2.844	0.020	12.11	0.12	0.972	0.005	1.060	0.015	0.713	0.007	0.755	0.008	288
SPMS4050	45	3.046	0.021	13.29	0.13	0.957	0.005	1.019	0.014	0.695	0.007	0.708	0.007	277
SPMS5059	54.5	2.958	0.021	13.12	0.13	0.968	0.005	0.980	0.014	0.684	0.007	0.670	0.007	266
SPVF0010	5	2.644	0.019	10.22	0.10	0.973	0.005	1.070	0.015	0.784	0.008	0.839	0.008	349
SPVF1020	15	2.799	0.020	12.29	0.12	0.966	0.005	1.009	0.014	0.691	0.007	0.698	0.007	318
SPVF2030	25	2.746	0.019	12.23	0.12	0.996	0.005	0.992	0.014	0.681	0.007	0.675	0.007	258
SPVF3040	35	3.022	0.021	12.66	0.13	1.019	0.005	0.951	0.013	0.724	0.007	0.689	0.007	219
SPVF4050	45	3.106	0.022	12.71	0.13	1.061	0.005	0.928	0.013	0.742	0.007	0.688	0.007	208
SPVF5060	55	3.209	0.022	13.34	0.13	1.072	0.005	0.903	0.013	0.730	0.007	0.659	0.007	182
SPVF6067	63.5	3.152	0.022	13.30	0.13	1.058	0.005	0.920	0.013	0.719	0.007	0.661	0.007	191
DC1-8	115	3.134	0.022	15.23	0.15	0.995	0.005	1.003	0.014	0.624	0.006	0.626	0.006	179
DC1-26	620	3.026	0.021	14.71	0.15	0.997	0.005	1.004	0.014	0.624	0.006	0.627	0.006	172

(^{234}U/^{238}U) activity ratios calculated from measured ^{234}U/^{235}U isotopic ratios assuming that ^{238}U/^{235}U = 137.88 and using the following decay constant: $\lambda_{238} = 1.551\times10^{-10}$ yr^{-1} and $\lambda_{234} = 2.826\times10^{-6}$ yr^{-1}(Akovali, 1994; Cheng et al., 2000). Analytical uncertainties are 0.5%. (^{230}Th/^{232}Th) activity ratios calculated from measured ^{232}Th/^{230}Th isotopic ratios using $\lambda_{232} = 4.948\times10^{-11}$ yr^{-1} and $\lambda_{230} = 9.158\times10^{-6}$ yr^{-1} (Cheng et al., 2000). Analytical precisions are 1% for the (^{230}Th/^{232}Th) activity ratios, 1% for the (^{238}U/^{232}Th) activity ratios and result in 1.4% for the (^{230}Th/^{238}U) activity ratios. Zr concentrations are from Jin et al. (2010). 'a' indicates activity ratio.

generally upward-decreasing values of (^{234}U/^{238}U) (Fig. 3a, b, c). (^{230}Th/^{238}U) ratios in the SPRT, SPMS, and SPVF profiles range from 1.036 to 1.052, from 0.980 to 1.096, and from 0.920 to 1.070, respectively (Table 1, Fig. 2). These values increase gradually towards the surface, displaying an opposite trend compared to the (^{234}U/^{238}U) activity ratios (Fig. 3d, e, f). Indeed, (^{234}U/^{238}U) and (^{230}Th/^{238}U) ratios for SSHO samples show a strong anti-correlation (Fig. 2). (^{230}Th/^{232}Th) ratios in the SPRT, SPMS, and SPVF profiles range from 0.692 to 0.701, from 0.670 to 0.755, and from 0.659 to 0.839, respectively (Table 1).

3.2. U and Th concentrations

Measured U and Th concentrations in all regolith samples range from 2.64 to 3.21 ppm and 12.11 to 13.34 ppm, respectively, values that are generally lower than the range in bedrock concentrations (3.03 to 3.13 ppm and 14.71 to 15.23 ppm, Table 1).

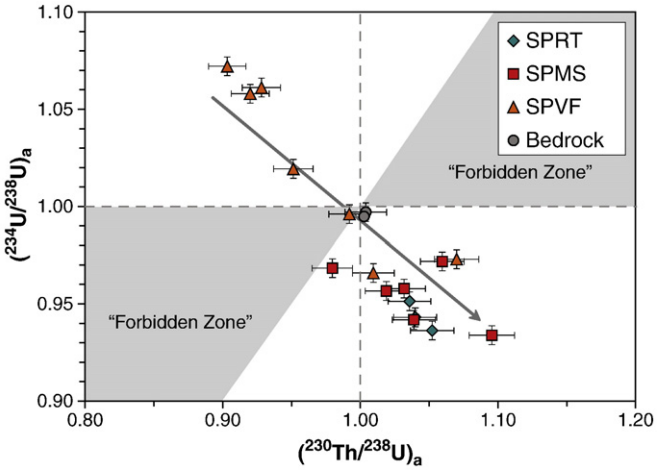

Fig. 2. Measured (^{234}U/^{238}U) and (^{230}Th/^{238}U) activity ratios for regolith samples from the south planar ridge top (SPRT), the south planar middle slope (SPMS), the south planar valley floor (SPVF), and two bedrock samples from DC-1. Grey area indicates the so-called "Forbidden Zone" (e.g., Dequincey et al., 2002). SSHO samples generally plot outside of the "forbidden zone". The arrow indicates the general evolution of regolith samples with depths moving towards the surface, consistent with a dual process of both gain and loss of U-series isotopes and mobility of ^{234}U>^{238}U>^{230}Th (see text).

To evaluate the loss or gain of elements in a weathering profile (especially to correct for the effects of regolith expansion/compaction and for relative concentration changes due to changes of other elements in the regolith), concentration (C) of an immobile (i.e. conservative) element i is commonly used to compare with the relative loss or gain of a more mobile element (j) by calculating the mass transfer coefficient $\tau_{i,j}$ (e.g., Brimhall and Dietrich, 1987):

$$\tau_{i,j} = \frac{C_{j,w}}{C_{j,p}} \cdot \frac{C_{i,p}}{C_{i,w}} - 1 \quad (1)$$

Positive $\tau_{i,j}$ values indicate the extent of enrichment of element j and negative values define the fractional depletion. A value of zero means that element j is as immobile in the weathered regolith (w) as the assumed immobile element i with respect to parent material (p). Elements that are commonly immobile in soils include Zr, Ti and Nb (Brimhall and Dietrich, 1987; Chadwick et al., 1990; Taylor and Blum, 1995; White et al., 1996; Price et al., 2005).

To calculate τ values for the SSHO regolith, we used the same parent composition as we assumed previously (Jin et al., 2010), i.e., the average of concentrations of core material (DC1) drilled in northern ridge top sampled between 0.3 m and 20 m. Previous study at SSHO has identified Zr, which has been observed to occur in the relatively insoluble and stable mineral zircon in the Rose Hill shale, to be the most immobile element in the analyzed regolith samples (Jin et al., 2010).

The calculated $\tau_{Zr,j}$ values for ^{238}U and ^{232}Th are shown in Figs. 4 and 5. For all regolith samples, $\tau_{Zr,U}$ values vary from 0.00 to −0.57 and decrease generally towards the surface (Fig. 4). All $\tau_{Zr,Th}$ values range from −0.14 to −0.66, also decreasing gradually towards the surface (Fig. 5).

4. Discussion

4.1. Mobility of ^{238}U and ^{232}Th during regolith formation

$\tau_{Zr,U}$ values show depletion profiles (Brantley and White, 2009) for all three cores along the planar transect at SSHO (Fig. 4). Thus, as bedrock dissolves and disaggregates to form regolith, U is readily released and lost, consistent with the notion that U is mobile under near-surface environments. Surprisingly, $\tau_{Zr,Th}$ values also show depletion

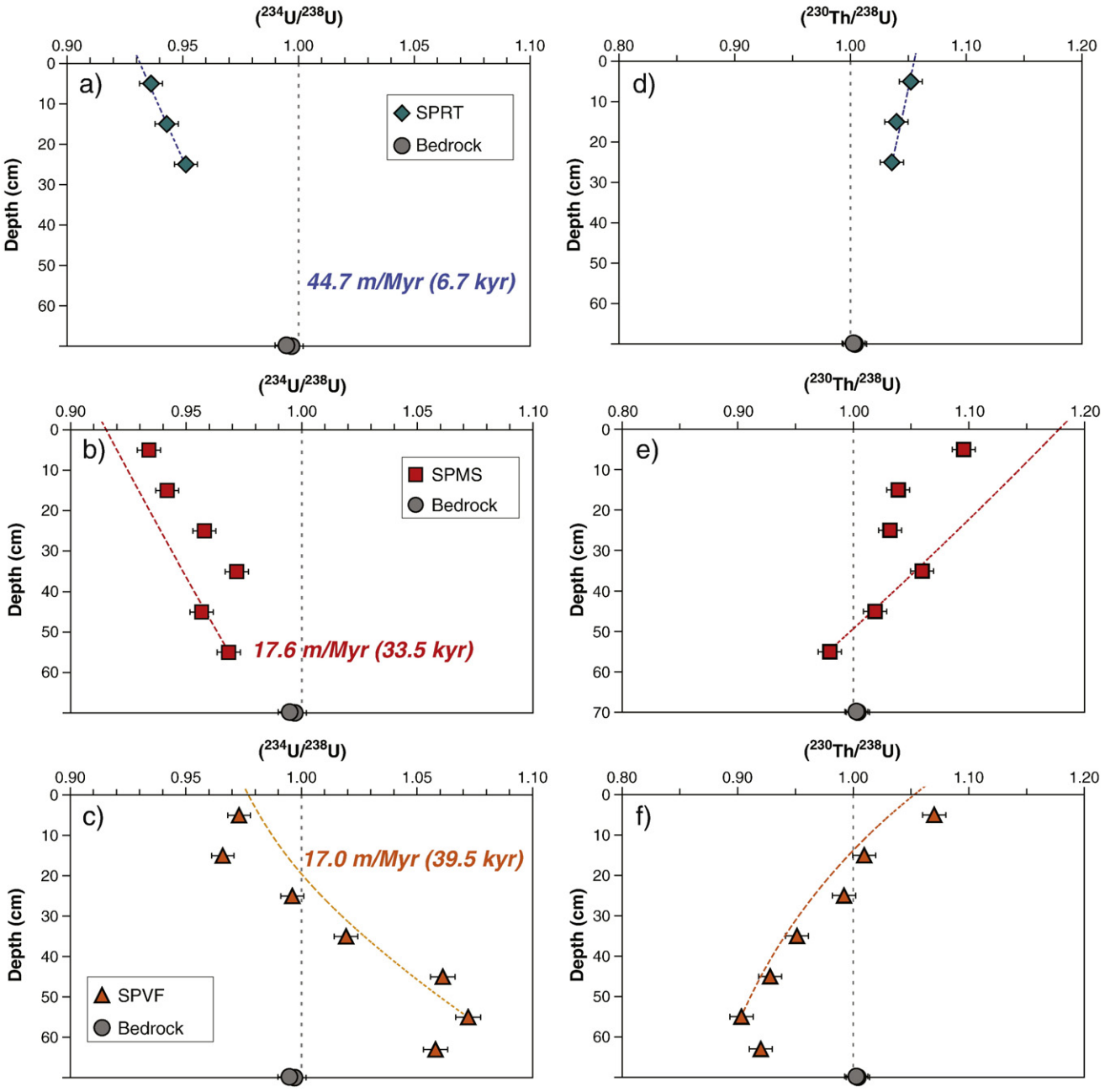

Fig. 3. Measured ($^{234}U/^{238}U$) and ($^{230}Th/^{238}U$) activity ratios for regolith samples from the ridge top profile (SPRT), the middle slope profile (SPMS), and the valley floor profile (SPVF) plotted against regolith depth. ($^{234}U/^{238}U$) and ($^{230}Th/^{238}U$) activity ratios of the two DC-1 bedrock samples are also shown. Dashed lines indicate ($^{234}U/^{238}U$) and ($^{230}Th/^{238}U$) activity ratios as a function of regolith depth calculated with parameters from Table 2 for each regolith profile using the model described in the text. Regolith production rates and residence times (in parentheses) for each profile are indicated. For each profile, the regolith depth is approximately 5 cm deeper than the deepest symbol.

profiles (Fig. 5). Normally, Th is immobile and particle-reactive during water–rock interaction due to the extremely low solubility of Th-containing phases (e.g., Rosholt et al., 1966; Latham and Schwarcz, 1987a,b; Gascoyne, 1992; Chabaux et al., 2003a). However, the negative τ_{ZrTh} values at SSHO indicate significant loss of Th during regolith formation. The extent of Th loss is similar to and sometimes greater than U (Figs. 4 and 5).

Enhancement of Th mobility during weathering could be partly explained by the presence of dissolved organic acids in the shallow soil profiles and formation of soluble Th-organic complexes or colloids (Langmuir and Herman, 1980; Chabaux et al., 2008). Such an increased Th mobility due to organic matter has been previously documented in studies of organic-rich river waters (e.g., Viers et al., 1997). Indeed, at SSHO, dissolved organic carbon in soil water collected from lysimeters along the southern transect has been shown to vary from about 0.9 to 28 ppm (unpub. data), within the range that could significantly increase Th solubility in water (Langmuir and Herman, 1980).

Furthermore, similar depletion profiles are observed for the major elements Mg, K, Al, Fe, and Si in these regolith samples (Jin et al., 2010). Based on these regolith data and on stream chemistry data at SSHO, Jin et al. (2010) suggested that the transformation of illite and "chlorite" to vermiculite and kaolinite is accompanied by loss of micron-sized particles. They concluded that Mg, K, and some of the Si are released to the stream as solutes, but the less soluble elements Al and Fe are lost predominantly through sub-surface transport of particles larger than 1.3 μm, i.e. particles that were filtered out by suction lysimeters (Jin et al., 2010). The observations are consistent

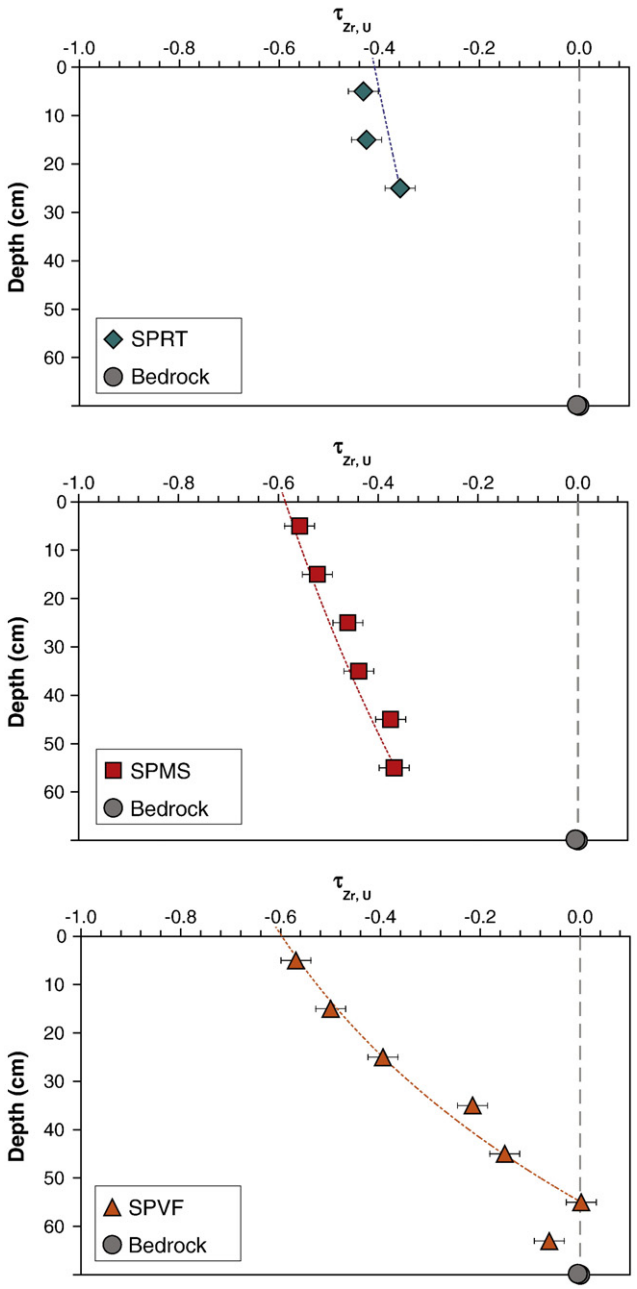

Fig. 4. Calculated τ values of ^{238}U with Zr as reference immobile element for regolith samples from SPRT, SPMS and SPVF. To complete the τ calculations, a composition of unaltered parent material was determined from the average of samples drilled at DC-1 as described previously (Jin et al., 2010). Errors in τ include the uncertainties of measured U and Zr concentrations as well as the error incurred due to heterogeneity of parent material (Jin et al., 2010). Dashed lines indicate $\tau_{Zr,U}$ values calculated using the model with parameters from Table 2 for each profile (see text for details).

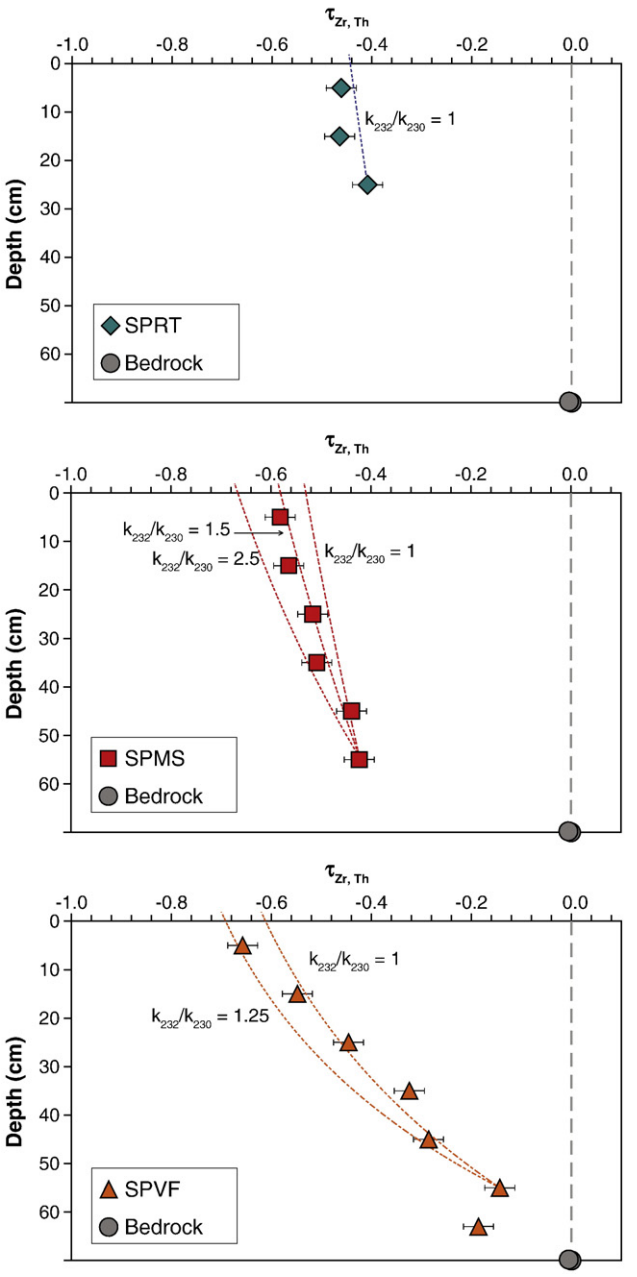

Fig. 5. Calculated τ values of ^{232}Th with Zr as reference immobile element for regolith samples from SPRT, SPMS, and SPVF. Dashed lines indicate $\tau_{Zr,Th}$ values as a function of depth calculated with parameters from Table 2 for each profile, and lines calculated with different k_{232}/k_{230} ratios are indicated (see text for details).

with loss of particles of secondary kaolinite or Fe + Al + Si-oxyhydroxides, presumably also containing organic material. This mechanism could explain the observed Th depletion profiles if Th were released during weathering of clay minerals but re-adsorbed onto particles. Given that relatively limited overland flow has been observed in the catchment (Qu and Duffy, 2007), the fine particles are thought to be translocated by flowing soil waters. Indeed, sub-surface particle transport is presumed to be promoted at SSHO because the field conditions are characterized by high infiltration rates, high soil moisture contents, and flow through macropores (Jin et al., 2010).

Furthermore, in these regolith samples, the mass loss of Th is strongly positively-correlated with the mass loss of Fe and Al ($R^2 = 0.98$), again consistent with fine particles or/colloids playing an important role for the observed Th loss. The loss of fine particles/colloids could also enhance U mobility above the mass loss of U as solute.

Values of $\tau_{Zr,U}$ and $\tau_{Zr,Th}$ in the deepest regolith samples of the SPRT and SPMS profiles do not reach zero at the regolith–bedrock interface (Figs. 4 and 5). Therefore, these samples have been significantly altered with respect to the parent bedrock. Such alteration at this depth was also observed as losses in major elements (Jin et al., 2010). Given that *rock fragments* sampled throughout the catchment from the bottom of profiles are compositionally similar to the average composition of parent bedrock, Jin et al. (2010) argued that the 10–20 cm thick layer lying directly below the regolith–bedrock interface is comprised of physically fractured but chemically unaltered shale together with chemically altered but difficult-to-sample sand/silt/clay. Thus, the bedrock–regolith interface defined

here by hand augering is a physical boundary to augering but not the chemical boundary defined by the lower limit of chemical weathering. Hypothetically, for example, the 10-cm layer just below augering at SPRT and SPMS sites could consist of ~60–80% rock fragments (observed in augered samples) identical to bedrock composition with 40–20% sand/silt/clay that is depleted 100% in Mg and K, ~60–90% in Fe, and ~80–100% in Al. When extrapolated versus depth, the depletion data are consistent with a depth to "bedrock" of ~1 m, where bedrock is now defined as lack of alteration in these elements. Of course, even at that depth the "bedrock" is not pristine: Jin et al. (2010) proposed that carbonate minerals may have dissolved to completion in the northern ridge top at 22 m depth and feldspar may begin dissolving at 6 m depth. Importantly, we note that the ($^{234}U/^{238}U$) ratio at 1 and 6 m as sampled in bedrock is at secular equilibrium as discussed in next section: we conclude that depth to bedrock that is chemically unaltered with respect to U coincides with the depth of bedrock chemically unaltered with respect to Mg, K, Fe, and Al.

4.2. Fractionation of ^{238}U, ^{234}U and ^{230}Th during regolith formation

In addition to the observed mass loss of U and Th, U-series activity ratios in regolith show significant fractionation from the two bedrock measurements (Figs. 2 and 3). Generally upward-decreasing values of ($^{234}U/^{238}U$) are exhibited in every profile (Fig. 3a, b, c). This pattern is consistent with the typical behavior of U-series isotopes observed during chemical weathering of profiles where duration of weathering increases upward and regolith mixing is minimal (e.g., Chabaux et al., 2003a, 2008). More loss of the lighter isotope of U from regolith is consistent with enhanced mobility due to the phenomenon of alpha decay. Although not measured here, fluids from early stages of chemical weathering have been observed to have ($^{234}U/^{238}U$)>1 in other natural systems as well as in leaching experiments (e.g., Chabaux et al., 2003a; Andersen et al., 2009). The observed trend of ($^{234}U/^{238}U$) ratios in these profiles is thus consistent with an increase in weathering intensity and duration towards the surface and rates of regolith mixing that are slow enough to not obscure weathering trends. Indeed, bioturbation is relatively ineffective in mixing the soils in New England where snow cover is significant (Kaste et al., 2007). Given the relatively similar climate, mixing processes may be slower than weathering for the SPRT, SPMS, and SPVF profiles at SSHO as argued previously for the major elements (Jin et al., 2010).

Unlike the bedrock sampled at 1 and 6 m depth, even the deepest regolith samples are characterized by ($^{234}U/^{238}U$) ratios that are at disequilibrium (Fig. 3a, b). This is consistent with the inference made based on the concentrations of U, Th, and major elements that the upper 1-meter interval or so of non-augerable bedrock underlying regolith is nonetheless chemically altered: values of τ for depleted elements returns to zero in SPRT and SPMS only at depths below the regolith–bedrock interface (Figs. 4 and 5). Furthermore, given that we have not observed significant depletion in Mg, K, Fe, and Al in the rock fraction in the deepest regolith samples or rock chips from the bedrock core (Jin et al., 2010), loss of ^{234}U is inferred to occur as rock fragments transform to sand/silt/clay. Jin et al. (2010) reported the bulk regolith samples exhibit BET surface area of about 25 m^2/g, whereas the surface area of the bedrock was presumably significantly lower. Therefore, based on the calculations above, the Rose Hill shale had to weather to produce at least 20% sand/silt/clay with this higher surface area to lose measurably significant amounts of ^{234}U than ^{238}U by direct ejection during alpha decay or due to incongruent dissolution.

In contrast to SPRT and SPMS, the deep regolith samples of the SPVF profile show ($^{234}U/^{238}U$) ratios greater than 1 (Fig. 3c). These high ratios are consistent with input of U with ($^{234}U/^{238}U$)>1 in the profile. Such gains of U in regolith have been documented in previous U-series studies such as in soil profiles from Africa and Australia (Dequincey et al., 2002; Chabaux et al., 2003b; Dosseto et al., 2008b), and in river sediments from Asia, South America, and Europe (Andersson et al., 1998; Dosseto et al., 2006a; Granet et al., 2007,2010). U inputs are also broadly consistent with the relatively soluble nature of U in the weathering environment (e.g., Chabaux et al., 2003a). For the sites described in previous studies, the U inputs are interpreted to reflect U that was precipitated or adsorbed from soil pore waters or from river waters that contain U characterized by ($^{234}U/^{238}U$)>1. Generally, the input of U has been attributed to co-precipitation or sorption of U in secondary Fe-hydroxides or clay minerals (Ames et al., 1983; Shirvington, 1983; Andersson et al., 1998; Duff et al., 2002; Chabaux et al., 2003a, 2008 and references therein). Similar processes could occur at SSHO as secondary Fe-hydroxides or clay minerals were observed to be common, especially in mid-slope and valley floor profiles (Jin et al., 2010).

($^{230}Th/^{238}U$) ratios in the SPRT, SPMS, and SPVF profiles increase gradually towards the surface, displaying an opposite trend compared to the ($^{234}U/^{238}U$) activity ratios (Fig. 3d, e, f). Such trends can be attributed to the differing behaviors of ^{230}Th and ^{238}U isotopes (Gascoyne, 1992): Th is less mobile, generally resulting in higher ($^{230}Th/^{238}U$) ratios (>1) in the residual weathering products and lower ($^{230}Th/^{238}U$) ratios (<1) in the weathering fluids (e.g., Vigier et al., 2001; Chabaux et al., 2003a; Dosseto et al., 2006a; Chabaux et al., 2008). While most of the regolith samples have ($^{230}Th/^{238}U$) ratios >1 as expected, a few deep regolith samples from the SPMS and SPVF profiles have ($^{230}Th/^{238}U$) activity ratios <1 (Fig. 3e, f). This observation is consistent with addition of U to the profiles as evidenced by the ($^{234}U/^{238}U$) activity ratios.

^{230}Th is less mobile compared to ^{238}U in these regolith samples (Fig. 3), which may appear contradictory to the overall mobile behavior of Th (and by inference, ^{232}Th) as documented by the trend of decreasing $\tau_{Zr,Th}$ values towards the surface. This latter trend indicates that the mobility of ^{232}Th is similar to that of ^{238}U during weathering in this system (Figs. 4 and 5). The different behaviors of ^{230}Th and ^{232}Th isotopes during regolith formation and the characteristic depletion profiles exhibited by U and Th will be further discussed in the following sections.

5. Model-derived regolith production rates and residence times

Determination of chemical weathering rates or residence times in a weathering profile from U-series disequilibrium relies on the use of a realistic model for U and Th mobility (e.g. Ghaleb et al., 1990; Scott et al., 1992; Vigier et al., 2001; Dequincey et al., 2002; Chabaux et al., 2003a; Maher et al., 2004; DePaolo et al., 2006; Chabaux et al., 2008; Dosseto et al., 2008b; Bourdon et al., 2009). At SSHO, ($^{234}U/^{238}U$) and ($^{230}Th/^{238}U$) ratios are consistent with increasing extent of weathering and increasing residence times upward in the profile. The mobility of isotopes decreases in the order $^{234}U>^{238}U>^{230}Th$. In addition to the loss of U-series isotopes due to chemical weathering and translocation of fine particles/colliods, some of the regolith profiles appear also to have gained U. Such a scenario is consistent with both gain and loss of U-series isotopes as observed in other systems (e.g., Dequincey et al., 2002).

5.1. Model description

We develop a model to interpret the data that is similar to the model of Dosseto et al. (2008b) developed for a weathering regolith profile in Australia. Similar approaches have been used to solve for residence times of river sediments in catchments around the world (e.g., Vigier et al., 2001, 2005, 2005, 2006; Dosseto et al., 2006a,b,c; Granet et al., 2007). The system of equations summarized below describes the three positions SPRT, SPMS, and SPVF as one-dimensional systems of upward moving regolith material. It is assumed that each site is experiencing an input of U-series isotopes that is constant at every depth. Only at the ridge top (SPRT) is the input rate of U-series isotopes equal to zero.

U in the Rose Hill shale is presumed to reside in the primary clay and Fe oxide minerals. The depth interval within which these U-

containing minerals react to measurable extent with chemically non-equilibrated meteoric water is defined as the U weathering reaction front. Assuming the arguments of Jin et al. (2010) are correct, the lower depths of the weathering fronts for feldspar and carbonate lie at ~6 and ~22 m respectively in the bedrock. Nonetheless, secular equilibrium still is apparently maintained across these reaction fronts. The implication is that only minimal interfacial area between water and U-containing clay/Fe-oxides develops at the carbonate and feldspar fronts. Thus, the measurable U weathering front is located approximately at about a meter depth where the sand/silt/clay fraction reaches approximately 20%: at that depth, Mg, K, Al, and Fe begin to show significant depletion as clay minerals start to chemically weather.

From the perspective of the land surface, our model is based upon the conceptualization of the U weathering front as a zone maintained at some depth through which regolith particles move "upward". During "ascent" of particles, the U-series isotopes are lost from the particle due to weathering and added due to sorption or co-precipitation reactions involving Fe-oxides, clay minerals, and fine particles/colloids. The mass conservation equations for ^{238}U, ^{234}U and ^{230}Th for each profile are then expressed as follows:

$$\frac{d^{238}\mathrm{U}}{dt} = \frac{F_{238}}{\lambda_{238}} - k_{238}{}^{238}\mathrm{U} - \lambda_{238}{}^{238}\mathrm{U} \quad (2)$$

$$\frac{d^{234}\mathrm{U}}{dt} = \frac{F_{234}}{\lambda_{234}} + \lambda_{238}{}^{238}\mathrm{U} - k_{234}{}^{234}\mathrm{U} - \lambda_{234}{}^{234}\mathrm{U} \quad (3)$$

$$\frac{d^{230}\mathrm{Th}}{dt} = \frac{F_{230}}{\lambda_{230}} + \lambda_{234}{}^{234}\mathrm{U} - k_{230}{}^{230}\mathrm{Th} - \lambda_{230}{}^{230}\mathrm{Th} \quad (4)$$

Here, F_{238}, F_{234}, and F_{230}, the input rates of ^{238}U, ^{234}U, and ^{230}Th, represent the processes that add U-series isotopes into profiles. These source terms, reported in activity per unit time (yr^{-2}), are considered to be constant with time (Ghaleb et al., 1990; Dequincey et al., 2002). F_{234}/F_{238} and F_{230}/F_{238} represent the (^{234}U/^{238}U) and (^{230}Th/^{238}U) activity ratios of the input sources, respectively.

The parameters k_{238}, k_{234}, and k_{230} are first-order rate constants (yr^{-1}) for release of ^{238}U, ^{234}U, and ^{230}Th from U- and Th-containing minerals (Latham and Schwarcz, 1987a,b; Plater et al., 1992; Vigier et al., 2001), i.e. it is assumed that U- and Th-containing phases dissolve at rates equal to $k_{238}{}^{238}$U, $k_{234}{}^{234}$U and $k_{230}{}^{230}$Th. λ_{238}, λ_{234}, and λ_{230} are the decay constants for ^{238}U, ^{234}U, and ^{230}Th (yr^{-1}); t is the residence time (yr) of particles in the zone where these elements weather. k_{234}/k_{238} and k_{230}/k_{238} describe the relative rates of loss of ^{234}U and ^{230}Th respectively to ^{238}U during leaching. Importantly, the ratio k_{234}/k_{238} documents the ratio of the release rate of ^{234}U due to phenomena related to alpha particle damage to the crystal lattice (k_{234}) compared to the release rate due to congruent dissolution of the mineral (k_{238}).

In a weathering profile, the average integrated regolith production rate P (m/Myr) can be expressed as the following equation:

$$P = \frac{h}{t} \quad (5)$$

where t corresponds to the duration for a particle moving from a reference position to its sample position and h is the vertical distance between these two positions (Appendix B).

For each regolith profile at SSHO, with the measured (^{234}U/^{238}U) and (^{230}Th/^{238}U) ratios as input values (the mass loss of U and Th are not used as input values), the unknown parameters (F_{238}, F_{234}, F_{230}, k_{238}, k_{234}, k_{230}, and P) can be fully solved by using the Matlab™ *lsqnonlin* function (Table 2, Appendix B). To eliminate the number of unknown parameters for simplicity and tractability of the model, we assume the unknown parameters (F_{238}, F_{234}, F_{230}, k_{238}, k_{234}, k_{230}) are constant over time for each weathering profile. Instead of solving for multiple t for individual samples within the profile, we also assume a constant production rate (P) for each profile. Thus, the derived production rate P represents an average rate over the duration of weathering for each profile. With the derived rate P, the total duration of weathering (residence time in regolith) for each profile is then calculated with Eq. (5) as discussed in Appendix B.

It is important to note that in the original model of Dequincey et al. (2002), both the U-series input and output terms were conceptualized as U carried as solutes. In fact, transport of fine particles along a hillslope might also play a role in transporting U-series isotopes as discussed here. In our model, we implicitly lump transport of solutes and particles together into the rate terms (F) and also into the leaching coefficients (k), because these chemical weathering mechanisms cannot be distinguished.

5.2. Model results

When the model is solved, the activity ratios (^{234}U/^{238}U) and (^{230}Th/^{238}U) are calculated as a function of regolith depth as shown in Fig. 3. The curves agree well with the measured ratios. The regolith production rates derived from the model decrease systematically with increasing distance from the ridge: ~45 m/Myr at SPRT, the highest point along the hillslope, ~18 m/Myr at SPMS, and ~17 m/Myr at SPVF (Table 2, Fig. 6). The duration of chemical weathering within the vertical regolith profile starting from the regolith–bedrock interface, termed here the apparent regolith residence time, increases significantly with distance away from the ridge, from ~7 kyr for the SPRT, to 34 kyr at the SPMS site, and to 40 kyr at the SPVF site (Table 2, Fig. 6). Notice that our model, based on vertical movement only, is only strictly applicable to SPRT. The residence time and regolith production rates at SPRT are thus easily interpreted. In contrast, the times calculated for SPMS and SPVF are the *apparent equivalent residence times* needed for a hypothetical particle to move vertically from the base to the top of regolith at those locations while establishing an equivalent U-series isotopic ratios as the real particle achieved while actually moving both vertically and downslope along the transect.

Model-derived k_{238} values vary from 1.4×10^{-5} to 3.0×10^{-5} yr^{-1} (Table 2), within the range of ^{238}U leaching coefficients derived from weathering profiles or river sediments with similar weathering time scales (Dosseto et al., 2008a). Model-derived k_{234}/k_{238} ratios from the three profiles are all greater than one, varying from 1.12 to 1.26 (Table 2), consistent with the fact that ^{234}U isotope is preferentially lost to the weathering fluids compared to ^{238}U (e.g., Fleischer, 1980). Such a range of values agrees well with many field and experimental studies of U isotopic fractionation during water–rock interaction (e.g., Vigier et al., 2001; Dequincey et al., 2002; Dosseto et al., 2008b; Andersen et al., 2009).

k_{230}/k_{238} ratios from the model range from 0.53 to 1.16 at SSHO (Table 2), indicating that ^{230}Th during weathering is generally less mobile than ^{238}U, but not completely immobile.

5.3. ^{238}U mass balance along the planar transect

Based on the model parameters (Table 2), the total ^{238}U input and output are calculated for each profile and increase down slope (Fig. 6). Here we calculate the ^{238}U mass balance for the 2D transect to test whether these ^{238}U fluxes could be U carried downslope by subsurface fluid flow and fine particles from SPRT to SPMS to SPVF (Fig. 6). This mass balance was not assumed in setting up the model.

To complete this check, we note that U input from wet precipitation is normally negligible (e.g., Chabaux et al., 2005). We also assume no significant U input from dust. Thus, U-series isotopes are lost through weathering and radioactive decay at the SPRT profile but no U is added. In contrast, the U input to the SPMS profile is calculated to be non-negligible by the model and we can check if it can be provided by the output calculated from SPRT. Similarly, the U output

Table 2
Regolith production rates, residence times, leaching coefficients, and U-series inputs derived from the model.

Sample profile	Regolith thickness (cm)	Regolith production rate (m/Myr)	Residence time (kyr)	k_{238} (10^{-5} yr^{-1})	k_{234}/k_{238}	k_{230}/k_{238}	$F_{238}/(\lambda_{238}^{238}U_0)$ (10^{-6} yr^{-1})	F_{234}/F_{238}	F_{230}/F_{238}
SPRT	30	44.7 ± 11.6	6.7	1.49 ± 0.35	1.26 ± 0.04	0.72 ± 0.08			
SPMS	59	17.6 ± 12.7	33.5	1.41 ± 1.55	1.12 ± 0.11	0.53 ± 0.34	0.31 ± 0.19	0.29 ± 0.39	2.59 ± 0.97
SPVF	67	17.0 ± 13.9	39.5	3.00 ± 1.65	1.16 ± 0.08	1.16 ± 0.05	1.15 ± 0.39	2.07 ± 1.04	5.64 ± 2.85

The model is solved multiple times to obtain 1000 sets of solutions for each profile as described in Appendix B. The model parameters are taken as the average of the sets of solution values and the uncertainties are calculated as the standard deviation on the sets of values. $^{238}U_0$ is initial number of ^{238}U atoms/g in the starting material of the system (Appendix B).

from SPMS is calculated to be non-negligible and it can be checked as an input to SPVF. Importantly, U inputs calculated by the model are accounted for with the U outputs from the site above (Fig. 6). This calculation demonstrates that no additional U input fluxes from deep groundwater or along-channel flow in the riparian zone at the valley floor.

5.4. Mobility of ^{238}U and ^{232}Th during regolith formation

By using model parameters (Table 2), the cumulative amount of ^{238}U that is lost through chemical weathering over time can be calculated (Eq. 2) (Fig. 4). The loss of ^{232}Th due to chemical weathering can be similarly calculated with the following equation:

$$\frac{d^{232}\mathrm{Th}}{dt} = \frac{F_{232}}{\lambda_{232}} - k_{232}{}^{232}\mathrm{Th} - \lambda_{232}{}^{232}\mathrm{Th} \quad (6)$$

where λ_{232} is the decay constant of ^{232}Th. Because no parameters of ^{232}Th are directly derived in the previous model, we assume here that the ^{232}Th leaching coefficient (k_{232}) is similar to that of ^{230}Th (k_{230}) just for modeling purposes. This latter value reflects the enhanced solubility due to the presence of organic complexes as well as loss of Th due to transport of fine particles. We calculate the value of F_{232} from model-derived F_{230} and average regolith $^{230}Th/^{232}Th$ for each profile, assuming that the transported Th is mainly in particle form.

Calculated τ values for ^{238}U from the model decrease gradually towards the surface and agree well with the observed loss of ^{238}U for the SPRT, SPMS and SPVF profiles (Fig. 4), consistent with our conceptual model that as regolith particles move "upward" in the profile, dissolution of clay minerals in shale gradually releases U into weathering fluids.

The τ values for ^{232}Th calculated from the model agree well with the observed loss of ^{232}Th for the SPRT, and for most of the SPVF profiles (Fig. 5), suggesting that similar to U, Th is also lost from the profile, probably by transport of both weathering fluids and fine particles. However, the SPMS and the uppermost SPVF profiles show more ^{232}Th depletion than the model predictions (Fig. 5). Such ^{232}Th depletion can be explained by using k_{232}/k_{230} ratios greater than 1, e.g., ranging from 1.25 to 2.5 (Fig. 5). These higher ratios are consistent with the presence of enhanced mobility of ^{232}Th relative to ^{230}Th for these uppermost samples.

Similarly, while the measured ($^{230}Th/^{232}Th$) ratios in SPRT and parts of the SPVF profiles agree well with the previous model calculations while assuming $k_{232}/k_{230}=1$, the measured ($^{230}Th/^{232}Th$) ratios in SPMS and uppermost SPVF profiles show higher values that can only be explained by using k_{232}/k_{230} ratios greater than 1 (Fig. 7). Because ^{230}Th is produced from ^{238}U and not necessarily associated with ^{232}Th-rich particles, such a change of $^{230}Th/^{232}Th$ ratios in the residual phases is consistent with a loss of ^{232}Th-rich particles (presumably with no ^{230}Th). Similar enhanced mobility due to preferential removal of ^{232}Th in different carrier phases has been previously reported in U-series studies: selective dissolution of minerals with high ^{232}Th concentrations has been suggested to explain the higher ($^{230}Th/^{232}Th$) ratios in the soils as compared to saprolite and bedrock in Australia (Dosseto et al., 2008b). Similarly, removal of detrital particles, i.e. the major carrier phase of ^{232}Th in Baltic seawater columns, has been proposed to account for a large increase of ($^{230}Th/^{232}Th$) in the Baltic seawater as compared to riverine inputs (Andersson et al., 1995; Porcelli et al., 2001).

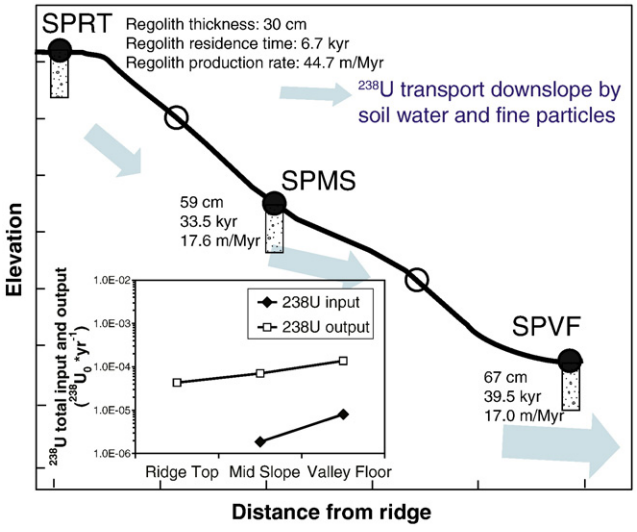

Fig. 6. a) Regolith thickness, residence time, and production rate calculated for the 2D planar transect at SSHO; b) Total input and output of ^{238}U for each profile along the 2D transect, calculated with the model-derived U input rates and leaching coefficients (Table 2). Total input and output are described in units of $^{238}U_0^* yr^{-1}$ where $^{238}U_0^*$ in this figure is the initial number of ^{238}U atoms in a 10 cm regolith column interval with a unit area.

5.5. Regolith production and duration of chemical weathering at SSHO

Previous studies report regolith formation rates on the order of 5 to ~100 m/Myr for a number of parent rock types, e.g., granodiorite and granite (Heimsath et al., 2000; Riebe et al., 2001, 2003, 2004a,b; Heimsath et al., 2005; Dosseto et al., 2008b), turbidite, sandstone and siltstone (Heimsath et al., 1997, 2001), and sedimentary and metamorphic rocks (Von Blanckenburg et al., 2004). Sedimentary rocks such as quartz-rich sandstones are generally less susceptible to alteration than igneous or metamorphic rocks, as they are already significantly weathered. This study shows however that the rate of formation of regolith and development of mineral–water interfacial area in the shale at SSHO occurs at a rather fast rate (17–45 m/Myr).

What controls these relatively fast regolith production rates? As observed by Jin et al. (2010), the deepest weathering reaction at SSHO is dissolution of ankerite, hypothesized to occur at 22 m below the surface. Above this at ~6 m below the surface lies the onset of the weathering front for feldspar dissolution. Based on arguments presented here, the onset of the weathering front of clay minerals (major U carrier phases) occurs within the upper meter below the bedrock–regolith interface. Porosity changes accompany chemical changes over these depths. Rock density data is consistent with an increase in porosity by 5% over the interval from 20 to 5 m depth. These changes are attributed partly to chemical weathering of carbonate minerals and feldspar and partly to ice-wedging from

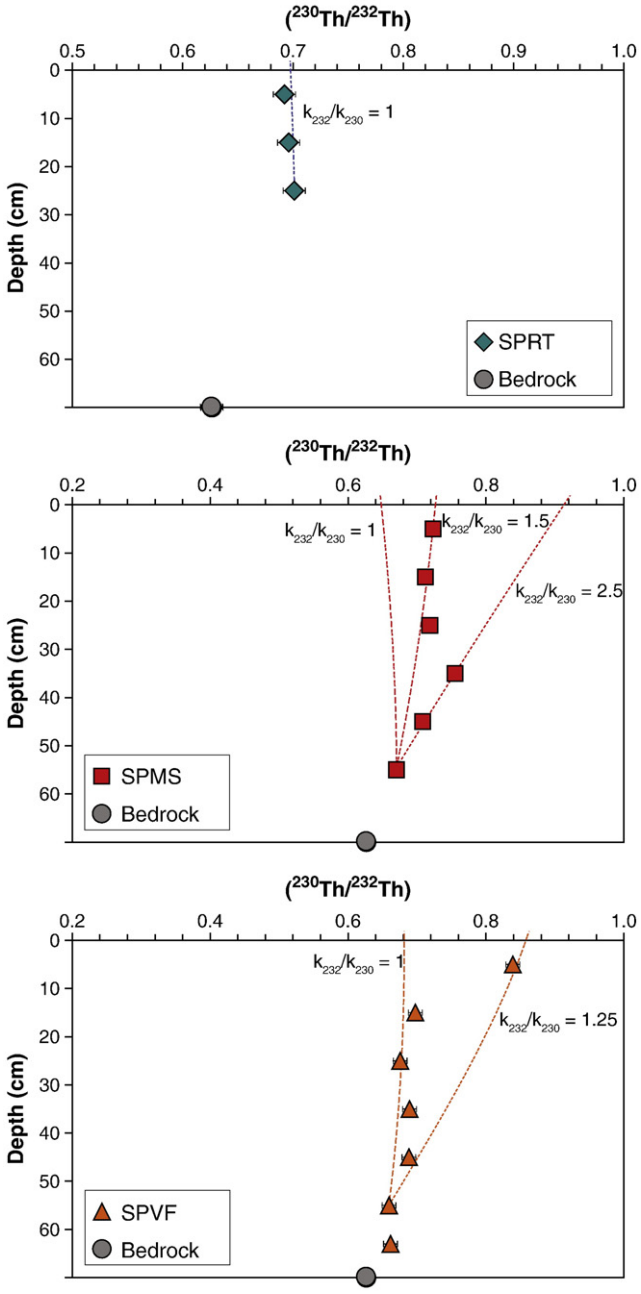

Fig. 7. Measured ($^{230}Th/^{232}Th$) activity ratios for regolith samples from a) SPRT, b) SPMS, and c) SPVF. ($^{230}Th/^{232}Th$) activity ratios of two DC-1 bedrock samples are also shown. Dashed lines indicate ($^{230}Th/^{232}Th$) activity ratios as a function of regolith depth calculated with parameters from Table 2; lines calculated with different k_{232}/k_{230} ratios are indicated (see text for details).

peri-glacial activities (Jin et al., 2010). Fracture-inducing reactions have been documented or hypothesized to accelerate the rates of weathering compared to non-fractured rocks for other systems (Fletcher et al., 2006; Buss et al., 2008; Brantley and White, 2009). We infer that increases in porosity due to fracturing, induced by chemical and physical factors, explain the relatively high regolith production rates at SSHO.

The surprisingly fast production rates of bedrock–regolith interface at SSHO are consistent with shale playing an important role in global elemental cycles and CO_2 consumption fluxes (Amiotte-Suchet et al., 2003). Thus, the wide distribution of shale worldwide and the ease of fracturing and high rate of particle loss of this rock type may accentuate the importance of shale in global weathering.

Regolith production rate at SPRT (~45 m/Myr) is significantly different from the production rates at SPMS and SPVF (~17 m/Myr). The regolith production rate at SPRT is also greater than the catchment-averaged erosion rate at SSHO (~15 m/Myr; Jin et al., 2010), perhaps suggesting that the regolith thickness is changing over time. These comparisons are consistent with the conclusion that the SSHO hillslope has not achieved steady state with respect to either regolith thickness or topography.

At SSHO, the regolith residence time increases with distance away from the ridge, from ~7 kyr for the SPRT, to 34 kyr at the SPMS site, and to 40 kyr at the SPVF site (Table 2). Despite the uncertainties in the regolith production rates, the SPMS and SPVF profiles each have duration of chemical weathering that is significantly longer than the SPRT profile. The last peri-glacial conditions at SSHO resulted from the advance of the late Wisconsinan Ice-sheet into Pennsylvania about ~27 kyr ago, changing to modern conditions ~15 kyr ago (Braun, 2005). Thus, the SPRT profile is characterized by regolith that formed more recently than the last peri-glacial period. By contrast, the model suggests that SPMS and SPVF profiles have some regolith that formed before the last peri-glacial period. The model is thus consistent with the presence of pre-glacial regolith that has not yet been completely removed, again consistent with lack of geomorphic steady state for this SSHO hillslope.

In contrast to these results, in the Mackenzie Basin of Northern Canada, duration of chemical weathering estimated from U-series disequilibrium in river sediments was relatively short compared to the time since the last glaciation (Vigier et al., 2001). In that case, it was inferred that glaciation completely removed the pre-existing weathering profile. However, such a "reset" effect was not observed at SSHO, presumably because of the difference in geographic locations: indeed, during the last glacial period, the Mackenzie Basin was completely covered by an ice-sheet in northern Canada and was characterized by high glacial erosion rates, whereas SSHO was in a peri-glacial environment with relatively lower erosion rates (Braun, 1989).

With increasing distance away from the ridge (Fig. 1a), the regolith production rates at SSHO decrease systematically with increasing regolith thickness (Table 2). Several time-dependent factors that control temporal variations in chemical weathering rates have been proposed, including reactive surface area, nature and saturation state of weathering fluids, and formation of secondary minerals (e.g., White and Brantley, 2003; Maher et al., 2004; Fletcher et al., 2006; Anderson et al., 2007; Maher, 2010). The change of these factors over time could potentially explain the inverse correlation between regolith production rate and residence time observed at SSHO. For example, a high dissolution rate is favored for a thin regolith cover with short residence time, such as at the ridge top of SSHO, because of the availability of fresh materials, large reactive surfaces, and water chemistry far away from solubility equilibrium with respect to the silicate minerals. In contrast, a low mineral dissolution rate is expected under a thick regolith cover with long residence time, e.g., for the valley floor site. Regolith chemistry and mineralogy studies at SSHO are consistent with slower mineral dissolution in the valley floor as compared to ridgetop (Jin et al., 2010).

5.6. Regolith production function at SSHO

The variation in regolith production rate as a function of regolith thickness at SSHO (Fig. 8) is consistent with an exponential function:

$$P = P_0 e^{-\alpha h} \tag{7}$$

Here P is the regolith production rate (m/Myr), h is the regolith thickness (cm), P_0 is the regolith production rate (m/Myr) with zero regolith thickness, and α is the depth scaling factor (cm^{-1}) (Fig. 8). Similar functions have been used in previous studies to describe the production rate of mobile soil from underlying saprolite (e.g., Cox, 1980;

Heimsath et al., 1997; Dietrich et al., 2003). The parameters in this function calculated from SSHO ($R^2 = 0.97$, $P_0 = 100.8$, $\alpha = 0.0279$) are compatible with those inferred for mobile soil production rates in California, Oregon, and Australia based on the measurements of cosmogenic isotopes (Heimsath et al., 1997, 2000, 2001; Dietrich et al., 2003). For instance, it has been shown that P_0 ranges from 50 to 2000 m/Myr, varying as a function of local lithology, climate, and tectonic uplift rates, whereas the depth scaling factors (α) lie within a narrow range from 0.02 to 0.04 cm^{-1} (Dietrich et al., 2003). Such a narrow range of depth scaling factors and the exponential mobile soil production function have been previously explained by the inference that the conversion of non-mobile to mobile soil is mainly controlled by the variation with depth of the effects of physical weathering and biogenic disturbances such as animal burrowing, tree throw, and rooting (Heimsath et al., 1997; Roering et al., 2002; Dietrich et al., 2003).

At SSHO, both the U-series and major element depth profiles (Jin et al., 2010) are consistent with a minimum of regolith mixing within the studied SSHO profiles, especially for the lower depths, as expected in regolith where bioturbation is relatively ineffective due to significant snow cover (Kaste et al., 2007). Rather, it is inferred for SSHO that chemical weathering processes and physical peri-glacial processes have significantly weakened and broken up the bedrock such that physical–chemical processes may dominate over biological processes in regolith production (e.g., Cox, 1980; Minasny and McBratney, 1999). Nonetheless, downslope movement of soil is known to occur due to tree throw throughout the catchment and at this point, the precise location of the lowermost limit of the "mobile soil layer" is not well defined in the context of the present study.

To derive the soil production rates with the cosmogenic approach requires an assumption that the thickness of the mobile soil layer in regolith is constant and the derived soil production rates correspond to the conversion rates of soils from the underlying immobile layer (Heimsath et al., 1997). In contrast, the regolith production function presented here is derived from the U-series isotopes where no such assumption is required (e.g., Dosseto et al., 2008b). This case study illustrates that U disequilibrium analysis provides a new and independent tool to quantify the regolith production function in weathering profiles. The regolith production rates can be envisioned here as the result of the downward advance of the U weathering front over time, and thus it provides time information for production of the lower part of the regolith. In fact, the derived production rates here are complementary to the soil production rates derived from the previous cosmogenic studies (e.g., Heimsath et al., 1997) and the combination of these two approaches will provide valuable information to elucidate the factors that control the rates and mechanisms of regolith formation.

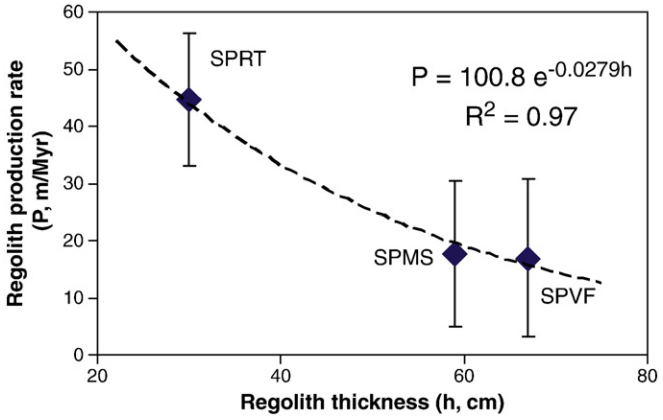

Fig. 8. Regolith production rates derived from the model plotted versus regolith thickness for three regolith profiles (SPRT, SPMS, and SPVF). Dashed line indicates the exponential fitted regolith production function.

6. Conclusions

To quantify regolith formation rates, we measured U-series isotopes (^{238}U, ^{234}U, and ^{230}Th) in three regolith profiles along a planar hillslope transect developed on shale bedrock in central Pennsylvania. Different from the bedrock, regolith samples show significant U-series disequilibrium and these activity ratios display depth trends consistent with the relative mobility of U and Th isotopes decreasing in the order $^{234}U > ^{238}U > ^{230}Th$. Depth profiles are explained by two processes: i) loss of U-series isotopes during water–rock interaction and ii) gain of U-series isotopes from upslope sites, e.g., U precipitated from circulating soil water and U and Th transported by particles.

Apparent equivalent regolith production rates calculated with U-series isotopes for these profiles decrease systematically from 45 m/Myr to 17 m/Myr, with increasing distance and regolith thickness from the ridge, suggesting that chemical weathering of shale at SSHO occurs actively at a rather fast rate. Regolith production rates at SSHO vary as an exponential function of regolith thickness. Apparent equivalent regolith residence times within these profiles range from 7 kyr to 40 kyr, increasing from the ridge to the valley floor. The presence of residence times longer than the last peri-glacial period (~15 kyr) may be consistent with lack of removal of pre-glacial regolith. Importantly, both chemical weathering reactions and sub-surface particle/colloid transport has been shown to contribute to mass losses of U and Th from the regolith at SSHO, as previously demonstrated for major elements (Jin et al., 2010).

For well-constrained field systems such as the hillslope studied here, the success of this method in estimating rates of regolith formation and duration of chemical weathering enhances our ability to use this technique in other environments to understand the response of regolith production to climate perturbations. The regolith production rates at SSHO also provide an important reference value for comparison to other critical zone observatories along both the lithology and climate gradients.

Acknowledgements

This work benefitted from reviews by A. Dosseto, G. Hilley, and an anonymous reviewer, and editorial handling by P. Delaney. Discussions with P. Stille, P. Bierman, H. Lin, A. Dere, T. White, K. Singha, E. Kirby and R. Slingerland are also acknowledged. We thank Z. Ruge and B. Ketchum for help with regolith sampling. Logistical support and/or data were provided by the NSF-supported Susquehanna/Shale Hills Critical Zone Observatory. Financial support was provided by National Science Foundation Grant CHE-0431328 to SLB for Center for Environmental Kinetics Analysis and Grant EAR-0725019 to C. Duffy (Penn State) for Susquehanna Shale Hills Critical Zone Observatory. SLB and LM were partially funded by Department of Energy Grant DE-FG02-05ER15675 to SLB. Funding from the Region Alsace, France and the Laboratory network "REALISE" for LHyGeS (EOST), University of Strasbourg and CNRS to FC is also acknowledged.

Appendix A. Analytical methods for U and Th isotopes

Samples consisted of all rock fragments, sand, silt, and clay recovered during augering. Bulk samples were air-dried and ground to pass through a 100-μm sieve. About 100 mg powdered samples were weighed and spiked with a mixed artificial ^{233}U–^{229}Th tracer for measurements of both U–Th isotopic compositions and concentrations. The samples were completely dissolved using a three-step procedure with HNO_3–HF, $HClO_4$, and HCl–H_3BO_3 acids.

U and Th separation and purification were performed by conventional ion exchange chromatography following procedures developed at the Laboratoire d'Hydrologie et de Geochimie de

Strasbourg (LHyGeS), University of Strasbourg (France) (e.g., Granet et al., 2007; Pelt et al., 2008). U concentrations and activity ratios, ($^{234}U/^{238}U$), were analyzed using ~70 ng U. The measurements were performed on a Thermal Ionization Mass Spectrometer (TIMS) Thermo-Scientific Triton. U concentrations were calculated using the measured $^{235}U/^{233}U$ isotopic ratios. ($^{234}U/^{238}U$) activity ratios were calculated using the analyzed $^{234}U/^{235}U$ ratios and assuming a constant $^{238}U/^{235}U$ ratio of 137.88, with the following decay constant: $\lambda_{238} = 1.551\times10^{-10}\,yr^{-1}$ and $\lambda_{234} = 2.826\times10^{-6}\,yr^{-1}$ (Akovali, 1994; Cheng et al., 2000). The precision and accuracy of the U activity ratios were determined from analyses of the HU1 standard solution and the BEN rock standards. Over the data acquisition period, the mean of the HU1-standard analyses of ($^{234}U/^{238}U$) is 1.001 ± 0.005 ($n=3$), was in good agreement with the laboratory 2008–2009 mean for ($^{234}U/^{238}U$) of 0.999 ± 0.005 ($n=32$; 2σ) and consistent with secular equilibrium. In addition, two analyses of the BEN rock standard, spiked with ^{233}U–^{229}Th tracer, yielded a mean ($^{234}U/^{238}U$) of 1.002 ± 0.002 and a mean U concentration of 2.465 ± 0.008 ppm, which are both consistent with the laboratory long-term mean values: ($^{234}U/^{238}U$) $=0.999\pm0.005$ ($n=5$; 2σ) and U $=2.457\pm0.013$ ($n=5$; 2σ), 2006–2009, and the reference values (U = 2.46 ppm; Govindaraju, 1994). The reproducibility of U concentrations and activity ratios by ID-TIMS was checked by duplicate analyses of 5 samples and is better than 0.5% and 0.4%, respectively.

$^{232}Th/^{230}Th$ isotopic ratios and Th concentrations were analyzed on ~600 ng Th with the TIMS Thermo-Scientific Triton. ^{230}Th and ^{229}Th were measured on the central SEM detector and ^{232}Th on a Faraday cup using the static collection mode. Th concentrations were determined using the measured $^{232}Th/^{229}Th$ isotopic ratios.

During the course of this study, the reproducibility of Th isotopic ratio measurements, checked by the in-house standard solution Th-105, is ~1% ($n=3$). In addition, the two analyses of the BEN rock standard, spiked with the ^{233}U–^{229}Th tracer, yielded a mean ($^{230}Th/^{238}U$) activity ratio of 1.004 ± 0.009 ($n=2$) and a mean Th concentration of 10.723 ± 0.079 ppm ($n=2$), which are consistent with secular equilibrium and the reference values (Th = 10.7 ppm; Govindaraju, 1994). The reproducibility of Th concentrations and activity ratios by ID-TIMS was checked by duplicate analyses of 4 samples and is better than 0.8% and 1.1%, respectively.

The total procedure blanks for U–Th isotopic and elemental analysis are about ~30–70 pg for U and ~180–420 pg for Th. They were negligible (<0.5‰) compared to the amount of U and Th analyzed in the studies samples. The ^{233}U–^{229}Th tracer was regularly calibrated by TIMS with the in-house AThO rock standard.

Appendix B. Solving the system of Eqs. (2)–(5)

We present here how we solved the system of Eqs. (2)–(5) for regolith production rate (P) or timescales of chemical weathering (t), input rates of ^{238}U, ^{234}U, ^{230}Th (F_{238}, F_{234}, F_{230}), and leaching rate constants (k_{238}, k_{234}, k_{230}). These values were derived to best reproduce the measured ($^{234}U/^{238}U$) and ($^{230}Th/^{238}U$) ratios as a function of depth.

Eqs. (2)–(4) were first solved analytically and the solutions were rearranged to describe ($^{234}U/^{238}U$) or ($^{230}Th/^{238}U$) for a weathering regolith sample as a function of F_{238}, F_{234}, F_{230}, k_{238}, k_{234}, k_{230}, and t (Eqs. (A1) and (A2)):

$$\left(\frac{^{234}U}{^{238}U}\right)_{activity} = \frac{\left(\frac{\lambda_{234}}{a_4-a_8} - \frac{\lambda_{234}F_{238}}{\lambda_{238}{}^{238}U_0 a_8(a_4-a_8)}\right)e^{-a_8 t} + \left(\left(\frac{^{234}U}{^{238}U}\right)_0 - \frac{\lambda_{234}}{a_4-a_8} - \frac{\lambda_{234}F_{238}}{\lambda_{238}{}^{238}U_0 a_4(a_4-a_8)} - \frac{F_{234}}{\lambda_{238}{}^{238}U_0 a_4}\right)e^{-a_4 t} + \frac{F_{234}}{\lambda_{238}{}^{238}U_0 a_4} + \frac{\lambda_{234}F_{238}}{\lambda_{238}{}^{238}U_0 a_4 a_8}}{\left(1-\frac{F_{238}}{\lambda_{238}{}^{238}U_0 a_8}\right)e^{-a_8 t} + \frac{F_{238}}{\lambda_{238}{}^{238}U_0 a_8}} \quad (A1)$$

$$\left(\frac{^{230}Th}{^{238}U}\right)_{activity} = \frac{Ae^{-a_8 t} + Be^{-a_4 t} + Ce^{-a_0 t} + \frac{\lambda_{230}\lambda_{234}F_{238}}{\lambda_{238}{}^{238}U_0 a_0 a_4 a_8} + \frac{\lambda_{230}F_{234}}{\lambda_{238}{}^{238}U_0 a_0 a_4} + \frac{F_{230}}{\lambda_{238}{}^{238}U_0 a_0}}{\left(1-\frac{F_{238}}{\lambda_{238}{}^{238}U_0 a_8}\right)e^{-a_8 t} + \frac{F_{238}}{\lambda_{238}{}^{238}U_0 a_8}} \quad (A2)$$

where

$$A = \frac{\lambda_{230}\lambda_{234}}{(a_0-a_8)(a_4-a_8)} - \frac{\lambda_{230}\lambda_{234}F_{238}}{\lambda_{238}{}^{238}U_0 a_8(a_4-a_8)(a_0-a_8)}$$

$$B = \frac{\lambda_{230}}{(a_0-a_4)}\left(\frac{^{234}U}{^{238}U}\right)_0 - \frac{\lambda_{230}\lambda_{234}}{(a_0-a_4)(a_4-a_8)} - \frac{\lambda_{230}F_{234}}{\lambda_{238}{}^{238}U_0 a_4(a_0-a_4)} - \frac{\lambda_{230}\lambda_{234}F_{238}}{\lambda_{238}{}^{238}U_0 a_4(a_0-a_4)(a_4-a_8)}$$

$$C = \left(\frac{^{230}Th}{^{238}U}\right)_0 - \frac{\lambda_{230}}{(a_0-a_4)}\left(\frac{^{234}U}{^{238}U}\right)_0 + \frac{\lambda_{230}\lambda_{234}}{(a_0-a_4)(a_4-a_8)} - \frac{\lambda_{230}\lambda_{234}}{(a_0-a_8)(a_4-a_8)} - \frac{F_{230}}{\lambda_{238}{}^{238}U_0 a_0} - \frac{\lambda_{230}F_{234}}{\lambda_{238}{}^{238}U_0 a_0 a_4} + \frac{\lambda_{230}F_{234}}{\lambda_{238}{}^{238}U_0 a_4(a_0-a_4)}$$
$$- \frac{\lambda_{230}\lambda_{234}F_{238}}{\lambda_{238}{}^{238}U_0 a_0 a_4 a_8} + \frac{\lambda_{230}\lambda_{234}F_{238}}{\lambda_{238}{}^{238}U_0 a_4 a_8(a_0-a_4)} - \frac{\lambda_{230}\lambda_{234}F_{238}}{\lambda_{238}{}^{238}U_0 a_8(a_0-a_4)(a_4-a_8)} + \frac{\lambda_{230}\lambda_{234}F_{238}}{\lambda_{238}{}^{238}U_0 a_8(a_0-a_8)(a_4-a_8)}$$

Here, we define
a_8 as $\lambda_{238}+k_{238}$;
a_4 as $\lambda_{234}+k_{234}$;
a_0 as $\lambda_{230}+k_{230}$;

($^{234}U/^{238}U$)$_0$ and ($^{230}Th/^{238}U$)$_0$ are initial activity ratios for the regolith sample; $^{238}U_0$ is the initial number of ^{238}U atoms in the starting material.

The derivation of Eq. (5) is based on the implicit assumption of isovolumetric weathering. At SSHO, volume strain has been calculated for some samples from regolith bulk density along the 2D transect (Jin et al., 2010). It has been shown that, although the regolith has expanded, the variation in strain is less than ~18% within the profile regolith volume from 17 to 54 cm. Only in the upper 3 cm layer has volume expanded significantly due to addition of organic matter (Jin et al., 2010). Future modeling efforts will explore the effect of this relatively modest non-isovolumetric weathering.

For each regolith profile, measured ($^{234}U/^{238}U$) and ($^{230}Th/^{238}U$) ratios in each sample are used to constrain the model. Instead of the measured bedrock samples (DC-1), the deepest sample from each profile was used to represent the starting material. To solve the model equations, we assume the unknown terms (F_{238}, F_{234}, F_{230}, k_{238}, k_{234}, and k_{230}) and the regolith production rate P are constant for each profile. Thus, the calculated value of P represents an average rate over the duration of weathering for each profile and the total duration of weathering is calculated with Eq. (5).

The model is constrained by 4 observations for SPRT ($^{234}U/^{238}U$ and $^{230}Th/^{238}U$ activity ratios for samples SPRT 0010 and 1020 as data points). Sample SPRT 2030 is used as the initial activity value of the starting material. The model fits 4 parameters (k_{238}, k_{234}, k_{230}, and P) to data describing the SPRT profile (we assume no U-series input sources for the ridge top site). The model for SPMS is constrained by 8 observations in the model (activity ratios for samples SPMS 0010, 1020, 2030, and 4050); and the activity ratios for SPMS5059 are used as the initial value of the starting material. The data from a depth of 35 cm, SPMS 3040, was not included in the model fit as it lies off the general trend of this profile (e.g., Fig. 2). The model calculated 7 parameters (F_{238}, F_{234}, F_{230}, k_{238}, k_{234}, k_{230}, and P) for the SPMS profile. The model is constrained by 10 observations for SPVF (activity ratios for SPVF 0010, SPVF1020, 2030, 3040, and 4050). The ratios for SPVF5060 were used as the initial value. SPVF6067 was not included in the calculation as it lies off the general trend of this profile (e.g., Fig. 2). Seven output parameters (F_{238}, F_{234}, F_{230}, k_{238}, k_{234}, k_{230}, and P) were derived for the SPVF profile. The number of model equations is equal to or greater than the number of unknowns, and thus the model is over-determined. The unknown parameters were solved in a similar manner to that of Dosseto et al. (2008b) as described below.

Best-fit parameters were calculated with the Matlab™ *lsqnonlin* function (version 7.1), which uses a large-scale algorithm to solve nonlinear least-squares problems. This function searches for the vector x that minimizes the sum of the square of the difference between observed and modeled values with a function $f(x)$ *which has m components of constraining equations*. The calculation is initiated with an initial value x_0, provided by the user. In this case, x is the vector of output parameters (F_{238}, F_{234}, F_{230}, k_{238}, k_{234}, k_{230}, and P) and the components of f are the measured ($^{234}U/^{238}U$) and ($^{230}Th/^{238}U$) activity ratios. The model calculates output parameters such that they fit the observed activity ratios within approximately 1%. The model calculation was performed 1000 times to obtain solutions for different random values for x_0. The average of these solutions and their standard deviations are presented in Table 2.

References

Akovali, Y.A., 1994. Nuclear data sheets for A = 234. Nucl. Data Sheets 71, 18.

Ames, L.L., McGarrah, J.E., Walker, B.A., 1983. Sorption of trace constituents from aqueous solutions onto secondary minerals. I Uranium. Clays Clay Miner. 31, 321–334.

Amiotte-Suchet, P., Probst, J., Ludwig, W., 2003. Worldwide distribution of continental rock lithology: implications for the atmospheric/soil CO_2 uptake by continental weathering and alkalinity river transport to the oceans. Glob. Biogeochem. Cycles 17, 1038. doi:10.1029/2002GB001891.

Amundson, R. (2004), Soil formation. In: Treatise on Geochemistry, H.D. Holland and K.K. Turekian (Eds in Chief). Elsevier Press, Amsterdam, pp. 1–35.

Andersen, M.B., Erel, Y., Bourdon, B., 2009. Experimental evidence for ^{234}U–^{238}U fractionation during granite weathering with implications for $^{234}U/^{238}U$ in natural waters. Geochim. Cosmochim. Acta 73, 4124–4141.

Anderson, S.P., Dietrich, W.E., Brimhall, G.H., 2002. Weathering profiles, mass-balance analysis, and rates of solute loss: linkage between weathering and erosion in a small, steep catchment. Geol. Soc. Am. Bull. 114, 1143–1158.

Anderson, S.P., von Blanckenburg, F., White, A.F., 2007. Physical and chemical controls on the Critical Zone. Elements 3, 315–319.

Andersson, P.S., Wasserburg, G.J., Chen, J.H., Papanastassiou, D.A., Ingri, J., 1995. ^{238}U–^{234}U and ^{232}Th–^{230}Th in the Baltic Sea and in river water. Earth Planet. Sci. Lett. 130, 217–234.

Andersson, P.S., Porcelli, D., Wasserburg, G.J., Ingri, J., 1998. Particle transport of ^{234}U–^{238}U in the Kalix River and in the Baltic Sea. Geochim. Cosmochim. Acta 62, 385–392.

Bierman, P.R., Nichols, K.K., 2004. Rock to sediment, slope to sea with ^{10}Be, rates of landscape change. Annu. Rev. Earth Planet. Sci. 32, 215–255.

Blackmer, G.C., Omar, G.I., Gold, D.P., 1994. Post-Alleghanian unroofing history of the Appalachian Basin, Pennsylvania, from apatite fission trace analysis and thermal models. Tectonics 13, 1259–1276.

Bourdon, B., Bureau, S., Andersen, M.B., Pili, E., Hubert, A., 2009. Weathering rates from top to bottom in a carbonate environment. Chem. Geol. 258, 275–287.

Brantley, S.L., 2008. Understanding soil time. Science 321, 1454–1455.

Brantley, S.L., White, T.S., Ragnarsdottir, K.V., 2007a. The Critical Zone: where rock meets life. Elements 3, 368.

Brantley, S.L., Godhaber, M.B., Ragnarsdottir, K.V., 2007b. Crossing disciplines and scales to understand the Critical Zone. Elements 3, 307–314.

Brantley, S.L., White, A.F., 2009. Approaches to modeling weathered regolith. Rev. Mineral. Geochem. 70, 435–484.

Braun, D.D., 1989. Glacial and periglacial erosion of the Appalachians. Geomorphology 2, 233–256.

Braun, D.D., 2005. Deglaciation of the Appalachian Plateau, northeastern Pennsylvania — till shadows, till knobs forming "beaded valleys": revisiting systematic stagnation-zone retreat. Geomorphology 75, 248–265.

Brimhall, G.H., Dietrich, W.E., 1987. Constitutive mass balance relations between chemical composition, volume, density, porosity, and strain in metosomatic hydrochemical systems: results on weathering and pedogenesis. Geochim. Cosmochim. Acta 51, 567–587.

Buss, H.L., Sak, P.B., Webb, S.M., Brantley, S.L., 2008. Weathering of the Rio Blanco quartz diorite, Luquillo Mountains, Puerto Rico: coupling oxidation, dissolution, and fracturing. Geochim. Cosmochim. Acta 72, 4488–4507.

Carson, M.A., Kirkby, M.J., 1972. Hillslope Form and Process. Cambridge Univ. Press, Cambridge.

Chabaux, F., Riotte, J., Dequincey, O., 2003a. U–Th–Ra fractionation during weathering and river transport. Rev. Mineral. Geochem. 52, 533–576.

Chabaux, F., Dequincey, O., Levesque, J.-J., Leprun, J.-C., Clauer, N., Riotte, J., Paquet, H., 2003b. Tracing and dating recent chemical transfers in weathering profiles by trace element geochemistry and ^{238}U–^{234}U–^{230}Th disequilibria: the example of the Kaya lateritic toposequence (Burkina-Faso). C. R. Geosci. 335, 1219–1231.

Chabaux, F., Riotte, J., Schmitt, A.-D., Carignan, J., Herckès, P., Pierret, M.-C., Wortham, H., 2005. Variations of U and Sr ratios in Alsace and Luxembourg rain waters: origin and hydrogeochemical implications. C. R. Geosci. 337, 1447–1456.

Chabaux, F., Granet, M., Pelt, E., France-Lanord, C., Galy, V., 2006. ^{238}U–^{234}U–^{230}Th disequilibria and timescale of sedimentary transfers in rivers: clues from the Gangetic plain rivers. J. Geochem. Explor. 88, 373–375.

Chabaux, F., Bourdon, B., Riotte, J., 2008. U-series geochemistry in weathering profiles, river waters and lakes. Radioact. Environ. 13, 49–104.

Chadwick, O.A., Brimhall, G.H., Hendricks, D.M., 1990. From a black to a grey box — a mass balance interpretation of pedogenesis. Geomorphology 3, 369–390.

Cheng, H., Edwards, R.L., Hoff, J., Gallup, C.D., Richards, D.A., Asmerom, Y., 2000. The half-lives of uranium-234 and thorium-230. Chem. Geol. 169, 17–33.

Copard, Y., Amiotte-Suchet, P., Di-Giovanni, C., 2007. Storage and release of fossil organic carbon related to weathering of sedimentary rocks. Earth Planet. Sci. Lett. 258, 345–357.

Cox, N.J., 1980. On the relationship between bedrock lowering and regolith thickness. Earth Surf. Processes 5, 271–274.

Drever, J.I., 2004. Surface and ground water, weathering, and soils. In: Holland, H.D., Turekian (Eds.), Treatise on Geochemistry, Volume 5. Elsevier. 626 pp.

DePaolo, D.J., Maher, K., Christensen, J.N., McManus, J., 2006. Sediment transport time measured with U-series isotopes: results from ODP North Atlantic drift site 984. Earth Planet. Sci. Lett. 248, 394–410.

Dequincey, O., Chabaux, F., Clauer, N., Sigmarsson, O., Liewig, N., Leprun, J.-C., 2002. Chemical mobilizations in laterites: evidence from trace elements and ^{238}U–^{234}U–^{230}Th disequilibria. Geochim. Cosmochim. Acta 66, 1197–1210.

Dietrich, W.E., Bellugi, D.G., Sklar, L.S., Stock, J.D., Heimsath, A.M., Roering, J.J., 2003. Geomorphic transport laws for predicting landscape form and dynamics. Prediction in Geomorphology. Geophysical Monograph 135. American Geophysical Union, pp. 1–30.

Dosseto, A., Bourdon, B., Gaillardet, J., Allegre, C.J., Filizola, N., 2006a. Timescale and conditions of chemical weathering under tropic climate: study of the Amazon basin with U-series. Geochim. Cosmochim. Acta 70, 71–89.

Dosseto, A., Turner, S.P., Douglas, G.B., 2006b. Uranium-series isotopes in colloids and suspended sediments: timescale for sediment production and transport in the Murray–Darling River system. Earth Planet. Sci. Lett. 246, 418–431.

Dosseto, A., Bourdon, B., Gaillardet, J., Allegre, C.J., Maurice-Bourgoin, L., 2006c. Weathering and transport of sediments in the Bolivian Andes: time constraints from uranium-series isotopes. Earth Planet. Sci. Lett. 248, 759–771.

Dosseto, A.D., Bourdon, B., Turner, S.P., 2008a. Uranium-series isotopes in river materials: insights into the timescales of erosion and sediment transport. Earth Planet. Sci. Lett. 265, 1–17.

Dosseto, A., Turner, S.P., Chappell, J., 2008b. The evolution of weathering profiles through time: new insights from uranium-series isotopes. Earth Planet. Sci. Lett. 274, 359–371.

Duff, M.C., Coughlin, J.U., Hunter, D.B., 2002. Uranium coprecipitation with iron oxide minerals. Geochim. Cosmochim. Acta 66, 3533–3547.

Duffy, C.J., Cusumano, J.M., 1998. A low-dimensional model for concentration-discharge in groundwater-stream systems. Water Resour. Res. 34, 2235–2247.

Fleischer, R.L., 1980. Isotopic disequilibrium of uranium: alpha-recoil damage and preferential solution effects. Science 207, 979–981.

Fletcher, R.C., Buss, H.L., Brantley, S.L., 2006. A spheroidal weathering model coupling porewater chemistry to soil thickness during steady-state denudation. Earth Planet. Sci. Lett. 244, 444–457.

Folk, R.L., 1960. Peterography and origin of the Tuscarora, Rose Hill, and Keefer Formations, Lower and Middle Silurian of eastern west Virginia. J. Sed. Petrol. 30, 1–58.

Gaillardet, J., 2008. Isotope geochemistry as a tool for deciphering kinetics of water–rock interaction. In: Brantley, S.L., Kubicki, J.D., White, A.F. (Eds.), Kinetics of Water–Rock Interaction. Springer, New York, pp. 591–653.

Gardner, T.W., Ritter, J.B., Shuman, C.A., Bell, J.C., Sasowsky, K.C., Pinter, N., 1991. A periglacial stratified slope deposit in the valley and ridge province of central

Pennsylvania, USA: sedimentology, stratigraphy, and geomorphic evolution. Permafrost Periglac. Process. 2, 141–162.
Gascoyne, M., 1992. Geochemistry of the actinides and their daughters. In: Ivanovich, M., Harmon, R.S. (Eds.), Uranium-Series Disequilibrium: Application to Earth, Marine, and Environmental Sciences. Oxford Sciences Publications, Oxford, pp. 34–61.
Ghaleb, B., Hillaire-Marcel, C., Causse, C., Gariepy, C., Vallieres, S., 1990. Fractionation and recycling of U and Th isotopes in a semiarid endoreic depression of central Syria. Geochim. Cosmochim. Acta 54, 1025–1035.
Godderis, Y., Roelandt, C., Schott, J., Pierret, M.-C., Francois, L.M., 2009. Towards an intergrated model of weathering, climate, and biospheric processes. Rev. Mineral. Geochem. 70, 411–434.
Govindaraju, K., 1994. Compilation of working values and sample description for 383 geostandards. Geostandards Newletter 18 (S1), 1–158.
Granet, M., Chabaux, F., Stille, P., France-Lanord, C., Pelt, E., 2007. Time-scales of sedimentary transfer and weathering processes from U-series nuclides: clues from the Himalayan rivers. Earth Planet. Sci. Lett. 261, 389–406.
Granet, M., Chabaux, F., Stille, P., Dosseto, A., France-Lanord, C., Blaes, E., 2010. U-series disequilibia in suspended river sediments and implication for sediment transfer time in alluvial plains : the case of the Himalayan rivers. Geochim. Cosmochim. Acta 74, 2851–2865.
Heimsath, A.M., Dietrich, W.E., Nishiizumi, K., Finkel, R.C., 1997. The soil production function and landscape equilibrium. Nature 388, 358–361.
Heimsath, A.M., Chappell, J., Dietrich, W.E., Nishiizumi, K., Finkel, R.C., 2000. Soil production on a retreating escarpment in southeastern Australia. Geology 28, 787–790.
Heimsath, A.M., Dietrich, W.E., Nishiizumi, K., Finkel, R.C., 2001. Stochastic processes of soil production and transport: erosion rates, topographic variation and cosmogenic nuclides in the Oregon coast range. Earth Surf. Process. Land. 26, 531–552.
Heimsath, A.M., Furbish, D.J., Dietrich, W.E., 2005. The illusion of diffusion: field evidence for depth-dependent sediment transport. Geology 33, 949–952.
Jin, L., Ravella, R., Ketchum, B., Bierman, P.R., Heaney, P., White, T., Brantley, S.L., 2010. Mineral weathering and elemental transport during hillslope evolution at the Susquehanna/Shale Hills Critical Zone Observatory. Geochim. Cosmochim. Acta 74, 3669–3691.
Kaste, J.M., Heimsath, A.M., Bostick, B.C., 2007. Short-term mixing quantified with fallout radionuclides. Geology 35, 234–246.
Kolowith, L.C., Berner, R.A., 2002. Weathering of phosphorus in black shales. Glob. Biogeochem. Cycles 16, 1140. doi:10.1029/2001GB001887.
Kump, L.R., Brantley, S.B., Arthur, M.A., 2000. Chemical weathering, atmospheric CO_2, and climate. Annu. Rev. Earth Planet. Sci. 28, 611–667.
Lal, D., 1991. Cosmic ray labeling of erosion surfaces: in situ nuclide production rates and erosion models. Earth Planet. Sci. Lett. 104, 424–439.
Langmuir, D., 1978. Uranium solution-mineral equilibria at low temperatures with applications to sedimentary ore deposits. Geochim. Cosmochim. Acta 42, 547–569.
Langmuir, D., Herman, J.S., 1980. The mobility of thorium in natural waters at low temperatures. Geochim. Cosmochim. Acta 44, 1753–1766.
Latham, A.G., Schwarcz, H.P., 1987a. On the possibility of determining rates of removal of uranium from crystalline igneous rocks using U-series disequilibria – 1: a U-leach model, and its applicability to whole-rock data. Appl. Geochem. 2, 55–65.
Latham, A.G., Schwarcz, H.P., 1987b. On the possibility of determining rates of removal of uranium from crystalline igneous rocks using U-series disequilibria – 2: applicability of a U-leach model to mineral separates. Appl. Geochem. 2, 67–71.
Lebedeva, M.I., Fletcher, R.C., Balashov, V.N., Brantley, S.L., 2007. A reactive diffusion model describing transformation of bedrock to saprolite. Chem. Geol. 244, 624–645.
Lin, H.S., 2006. Temporal stability of soil moisture spatial pattern and subsurface preferential flow pathways in the Shale Hills Catchment. Vadose Zone J. 5, 317–340.
Lin, H., Kogelmann, W., Walker, C., Bruns, M.A., 2006. Soil moisture patterns in a forested catchment: a hydropedological perspective. Geoderma 131, 345–368.
Littke, R., Klussmann, U., Krooss, B., Leythaeuser, D., 1991. Quantification of loss of calcite, pyrite, and organic matter due to weathering of Toarcian black shales and effects on kerogen and bitumen characteristics. Geochim. Cosmochim. Acta 55, 3369–3378.
Lynch, J.A., 1976. Effects of Antecedent Soil Moisture on Storm Hydrographs. University Park, Pennsylvania State University.
Lynch, J.A., and Corbett, E.S. (1985), Source-area variability during peak flow, edited by E.B. Jones and T.J. Ward, J. Irrig. Drain. Div. Am. Soc. Civ. Eng., pp. 300–307., in Watershed Management in the 1980s, E. Jones and T. Ward, Editors. ASCE: Reston, VA. p. 300–307.
Maher, K., 2010. The dependence of chemical weathering rates on fluid residence time. Earth Planet. Sci. Lett. 294, 101–110.
Maher, K., DePaolo, D.J., Lin, J.C.F., 2004. Rates of silicate dissolution in deep-sea sediment: in situ measurement using U-234/U-238 of pore fluids. Geochim. Cosmochim. Acta 68, 4629–4648.
Mathieu, D., Bernat, M., Nahon, D., 1995. Short-lived U and Th isotope distribution in a tropical laterite derived from Granite (Pitinga river basin, Amazonia, Brazil): application to assessment of weathering rate. Earth Planet. Sci. Lett. 136, 703–714.
Minasny, B., McBratney, A.B., 1999. A rudimentary mechanistic model for soil production and landscape development. Geoderma 90, 3–21.
Montgomery, D.R., 2007. Soil erosion and agricultural sustainability. Proc. Natl. Acad. Sci. U. S. A. 104 (33), 13268–13272.
Murphy, S.F., Brantley, S.L., Blum, A.E., White, A.F., Dong, H., 1998. Chemical weathering in a tropical watershed, Luquillo Mountains, Puerto Rico: II. Rate and mechanism of biotite weathering. Geochim. Cosmochim. Acta 62, 227–243.
National Oceanographic and Atmospheric Administration (NOAA) (2007), U.S. divisional and station climatic data and normals: Asheville, North Carolina, U.S. Department of Commerce, National Oceanic and Atmospheric Administration, National Environmental Satellite Data and Information Service, National Climatic Data Center, http://cdo.ncdc.noaa.gov/CDO/cdo.
Pelt, E., Chabaux, F., Innocent, C., Navarre-Sitchler, A.K., Sak, P.B., Brantley, S.L., 2008. Uranium–thorium chronometry of weathering rinds: rock alteration rate and paleo-isotopic record of weathering fluids. Earth Planet. Sci. Lett. 276, 98–105.
Petsch, S.T., Eglinton, T.I., Edwards, K.J., 2001. ^{14}C-dead living biomass: evidence for microbial assimilation of ancient organic carbon during shale weathering. Science 292, 1127–1131.
Piersson-Wickmann, A., Reisberg, L., France-Lanord, C., 2002. Behavior of Re and Os during low temperature alteration: results from Himalayan soils and altered black shales. Geochim. Cosmochim. Acta 66, 1539–1548.
Plater, A.J., Ivanovich, M., Dugdale, R.E., 1992. Uranium series disequilibrium in river sediments and waters: the significance of anomalous activity ratios. Appl. Geochem. 7, 101–110.
Plater, A.J., Dugdale, R.E., Ivanovich, M., 1994. Sediment yield determination using uranium-series radionuclides: the case of the Wash and Fenland drainage basin, eastern England. Geomorphology 11, 41–56.
Porcelli, D., Andersson, P.S., Baskaran, M., Wasserburg, G.J., 2001. Transport of U- and Th- series nuclides in a Baltic Shield watershed and the Baltic Sea. Geochim. Cosmochim. Acta 65, 2439–2459.
Porder, S., Vitousek, P.M., Chadwick, O.A., Page Chamberlin, C., Hilley, G.E., 2007. Uplift, erosion, and phosphorus limitation in terrestrial ecosystems. Ecosystems 10, 158–170.
Price, J.R., Velbel, M.A., Patino, L.C., 2005. Rates and time scales of clay-mineral formation by weathering in saprolitic regoliths of the southern Appalachians from geochemical mass balance. Geol. Soc. Am. Bull. 117, 783–794.
Qu, T., Duffy, C.J., 2007. A semi-discrete finite volume formation for multiprocess watershed simulation. Water Resour. Res. 43. doi:10.1029/2006WR005752.
Reuter, J., Bierman, P., Pavich, M., Gellis, A., Larsen, J., Finkel, R., 2004. Erosion of the Susquehanna River Basin: assessing relations between ^{10}Be-derived erosion rates and basin characteristics. Geological Society of America programs with abstracts.
Riebe, C.S., Kirchner, J.W., Granger, D.E., Finkel, R.C., 2001. Strong tectonic and weak climatic control of long-term chemical weathering rates. Geology 29, 511–514.
Riebe, C., Kirchner, J.W., Finkel, R.C., 2003. Long-term rates of chemical weathering and physical erosion from cosmogenic nuclides and geochemical mass balance. Geochim. Cosmochim. Acta 67, 4411–4427.
Riebe, C.S., Kirchner, J.W., Finkel, R.C., 2004a. Erosional and climatic effects on long-term chemical weathering rates in granitic landscapes spanning diverse climate regimes. Earth Planet. Sci. Lett. 224, 547–562.
Riebe, C.S., Kirchner, J.W., Finkel, R.C., 2004b. Sharp decrease in long-term chemical weathering rates along an altitudinal transect. Earth Planet. Sci. Lett. 218, 421–434.
Roden, M.K., Miller, D.S., 1989. Apatite fission-track thermochronology of the Pennsylvania Appalachian Basin. Geomorphology 2, 39–51.
Roering, J., Almond, P., Tonkin, P., McKean, J., 2002. Soil transport drived by biological processes over millennial time scales. Geology 30, 1115–1118.
Rosholt, J., Doe, B., Tatsumoto, M., 1966. Evolution of the isotopic composition of uranium and thorium in soil profiles. Geol. Soc. Am. Bull. 77, 987–1004.
Scott, R.D., MacKenzie, A.B., Alexander, W.R., 1992. The interpretation of ^{238}U–^{234}U–^{230}Th–^{226}Ra disequilibria produced by rock–water interactions. J Geochem Explor 45, 323–343.
Shirvington, P.J., 1983. Fixation of radionuclides in the ^{238}U decay series in the vicinity of mineralized zones: 1. The Austatom Uranium Prospect, Northern Territory, Australia. Geochim. Cosmochim. Acta 47, 403–412.
Small, E.E., Anderson, R.S., Hancock, G.S., 1999. Estimates of the rate of regolith production using ^{10}Be and ^{26}Al from an Alpine hillslope. Geomorphology 27, 131–150.
Stallard, R.F., 1992. Tectonic processes, continental freeboard, and the rate-controlling step for continental denudation. In: Butcher, S.S., Charlson, R.J., Orians, G.H., Wolfe, G.V. (Eds.), Global Biogeochemical Cycles. Academic Press, London, pp. 93–121.
Steefel, C.I., 2008. Geochemical kinetics and transport. In: Brantley, S.L., Kubicki, J.D., White, A.F. (Eds.), Kinetics of Water–Rock Interaction. Springer, New York, pp. 545–589.
Taylor, A., Blum, J.D., 1995. Relation between soil age and silicate weathering rates determined from the chemical evolution of a glacial chronosequence. Geology 23, 979–982.
Tuttle, M.L.W., Breit, G.N., 2009. Weathering of the New Albany Shale, Kentucky, USA: I. weathering zones defined by mineralogy and major-element composition. Appl. Geochem. 24, 1549–1564.
Tuttle, M.L.W., Breit, G.N., Goldhaber, M.B., 2009. Weathering of the New Albany Shale, Kentucky: II. Redistribution of minor and trace elements. Appl. Geochem. 24, 1565–1578.
Viers, J., Dupre, B., Polve, M., Schott, J., Dandurand, L., Braun, J.J., 1997. Chemical weathering in the drainage basin of a tropical watershed (Nsimi-Zoetele site, Cameroon): comparison between organic-poor and organic-rich waters. Chem. Geol. 140, 181–206.
Vigier, N., Bourdon, B., Turner, S., Allegre, C.J., 2001. Erosion timescales derived from U-decay series measurements in rivers. Earth Planet. Sci. Lett. 193, 485–499.
Vigier, N., Bourdon, B., Turner, S., Van Calsteren, P., Subramanian, V., Dupre, B., Allegre, C.J., 2005. Parameters influencing the duration and rates of weathering deduced from U-series measured in rivers: the Deccan trap region (India). Chem. Geol. 219, 69–91.
Vigier, N., Burton, K.W., Gislason, S.R., Rogers, N.W., Duchene, S., Thomas, L., Hodge, E., Schaefer, B., 2006. The relationship between riverine U-series disequilibria and erosion rates in a basaltic terrain. Earth Planet. Sci. Lett. 249, 258–273.
Von Blanckenburg, F., 2005. The control mechanisms of erosion and weathering at basin scale from cosmogenic nuclides in river sediment. Earth Planet. Sci. Lett. 237, 462–479.
Von Blanckenburg, F., Hewawasam, T., Kubik, P., 2004. Cosmogenic nuclide evidence for low weathering and denudation in the wet tropical Highlands of Sri Lanka. J. Geophys. Res. 109, F03008. doi:10.1029/2003JF000049.
White, A.F., Blum, A.E., 1995. Effects of climate on chemical weathering in watersheds. Geochim. Cosmochim. Acta 59, 1729–1747.

White, A.F., Blum, A.E., Marjorie, S., Schulz, M.S., Bullen, T.D., Harden, J.W., Peterson, M.L., 1996. Chemical weathering rates of a soil chronosequence on granitic alluvium: I. Quantification of mineralogical and surface area changes and calculation of primary silicate reaction rates. Geochim. Cosmochim. Acta 60, 2533–2550.

White, A.F., Blum, A.E., Schlz, M.S., Vivit, D.V., Stonestrom, D.A., Larsen, M., Murphy, S.F., Eberl, D., 1998. Chemical weathering in a tropical watershed, Luquillo Mountains, Puerto Rico: I. long-term versus short-term weathering fluxes. Geochim. Cosmochim. Acta 62, 209–226.

White, A.F., Brantley, S.L., 2003. The effect of time on the weathering of silicate minerals: why do weathering rates differ in the laboratory and field? Chem. Geol. 202, 479–506.

Wilkinson, B.H., McElroy, B.J., 2007. The impact of humans on continental erosion and sedimentation. Geol. Soc. Am. Bull. 119, 140–156.

Yoo, K., Amundson, R., Heimsath, A.M., Dietrich, W.E., Brimhall, G.H., 2007. Integration of geochemical mass balance with sediment transport to calculate rates of soil chemical weathering and transport on hillslopes. J. Geophys. Res. 112, F02013. doi:10.1029/2005JF000402.